Dalton Transactions

Accepted Manuscript

This article can be cited before page numbers have been issued, to do this please use: E. Garcia-Moreno, A. Tomas, E. Atrian Blasco, S. Gascon, E. Romanos, M. J. Rodriguez-Yoldi, E. Cerrada and M. Laguna, *Dalton Trans.*, 2015, DOI: 10.1039/C5DT01802A.

ROYAL SOCIETY OF CHEMISTRY

www.rsc.org/dalton

View Article Online
DOI: 10.1039/C5DT01802A

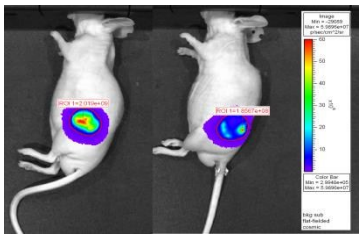

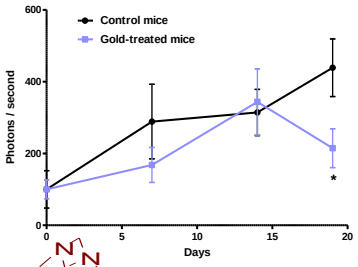

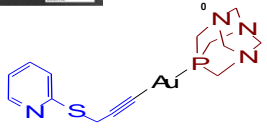

View Article Online
DOI: 10.1039/C5DT01802A

Journal Name

ARTICLE

Received 00th January 20xx,

Accepted 00th January 20xx

DOI: 10.1039/x0xx00000x

www.rsc.org/

In vitro and *in vivo* evaluation of organometallic gold (I) derivatives as anticancer agents.

Elena García-Moreno[a], Alejandro Tomás[a], Elena Atrián-Blasco[a], Sonia Gascón[b], Eduardo Romanos[c], Mª Jesus Rodriguez-Yoldi[b], Elena Cerrada[a] and Mariano Laguna[a,*]

Alkyne gold (I) derivatives with the water soluble phosphanes PTA (1,3,5-triaza-7-phosphaadamantane) and DAPTA (3,7-diacetyl-1,3,7-triaza-5-phosphabicyclo[3.3.1]nonane) were described and their anticancer potential against colon cancer cell lines Caco-2 (PD7 and TC7 clones) were studied. Strong antiproliferative effects are found, for all the new complexes, to be even more pronounced than for the reference drug cisplatin, and similar to auranofin. The interaction of these derivatives with bovine serum albumin (BSA) was studied by fluorescence spectroscopy. Types of quenching and binding constants were determined by fluorescence quenching method. Moderate values of the binding constant are calculated for the tested derivatives indicating that these complexes can be stored and carried easily by this protein in the body. The study of the thermodynamic parameters in the case of [Au(C≡CCH$_2$Spyridine)(PTA)] points out to the presence of van der Waals interactions or hydrogen bonding between the metallic complex and the protein. In addition, the complex [Au(C≡CCH$_2$Spyridine)(PTA)] has shown inhibition in colon cancer proliferation of HTC-116-luc2 cell lines via apoptotic pathway and S-phase arrest of the cell cycle. Intraperitoneal injection of this derivative in athymic nude mice inoculated with HTC-116-luc2 cells prolonged their survival and displayed moderate inhibition of the tumour growth with no subsequent organ (kidney and liver) damage after treatment.

Introduction

Platinum was the first metal used in the treatment of cancer since the accidental discovery of the antitumor properties of one of its coordination complexes, *cis*-diammine dichloroplatinum(II), known as *cisplatin*. Nowadays the use of this drug is on the decline as a result of an increased prescription of the second- and third-generation analogs: *carboplatin* (*cis*-diammine(1,1-cyclobutanedicarboxylato)platinum(II)) and *oxaliplatin* (*cis*-[oxalate(*trans-l*-1,2-diaminocyclohexane)platinum(II)])[1]. Both derivatives display much less oto and nephrotoxicity than cisplatin, although induction to peripheral neuropathy (toxicity for peripheral sensory nerves) is found in the latest drug. Precisely, the use of *oxaliplatin*, which is especially effective in combination with 5-fluorouracil and leuvocorin[2] against advanced colorectal cancer, is limited by these side effects[3]. These negative effects and the drug resistance (problem derived from a repeated exposure to the drug) in the cisplatin derivatives therapy have encouraged researchers to find alternatives to circumvent these undesirable effects.

Consequently, during the last years the interest in complexes with other metals for cancer chemotherapy has grown rapidly. Among the non-platinum compounds, ruthenium (II and III)[4-9], titanium (IV)[4, 10-12] and gold (I and III)[4, 9, 11, 13-26] are the most studied metals. Regardless of the high number of promising results for non-platinum metallic complexes in preclinical studies, only few compounds have been investigated in clinical phase I and phase II studies. In the case of titanium, budotitane (*cis*-diethoxybis(1-phenylbutane-1,3-dionato)titanium (IV) and titanocene dichloride (bis(cyclopentadienyl)titanium(IV) dichloride) have been investigated in clinical trials[27, 28] with low activities, probably due to their poor solubility in aqueous media and the poor stability of these compounds under physiological conditions[29]. Better results have been obtained for ruthenium derivatives. Thus, imidazolium-*trans*-[tetrachloro(DMSO)(imidazole) ruthenate(III)] (NAMI-A) was found to reduce metastasis in certain *in vivo* models of cancer[30], indazolium bisindazoletetrachlororuthenate (KP1019) was found to be active against colon cancer[31] and the ruthenium (II) complex [Ru(η^6-toluene)Cl$_2$(PTA)] (PTA = 1,3,5-triaza-7-phosphaadamantane) named RAPTA-T have shown antimetastatic effects *in vivo* in addition to anti-angiogenic properties[32, 33].

Moreover, organometallic compounds, considered as intermediates between classical inorganic and organic derivatives, have recently been studied and reviewed as potential anticancer drugs[14, 34-39] and some of them, mentioned above, have entered in clinical trials. Although most of the drugs used today are purely organic compounds, organometallic derivatives exhibit some advantages over organic drugs, which make them to be considered as possible candidates in anticancer treatment. Several properties of these compounds offer plenty of opportunities in the design of new

[a] *Departamento de Química Inorgánica, Instituto de Síntesis Química y Catálisis Homogénea-ISQCH, Universidad de Zaragoza-C.S.I.C., 50009 Zaragoza, Spain. E-mail: mlaguna@unizar.es and ecerrada@unizar.es*
[b] Departamento de Farmacología y Fisiología. Unidad de Fisiología, Facultad de Veterinaria, Universidad de Zaragoza, 50013, Zaragoza, CIBERobn, Spain.
[c] Instituto Aragonés de Ciencias de la Salud (IACS). Av San Juan Bosco 13, 50009, Zaragoza.
† Electronic Supplementary Information (ESI) available: [Stern-Volmer plots for the quenching of BSA with complexes 5-12]. See DOI: 10.1039/x0xx00000x

View Article Online
DOI: 10.1039/C5DT01802A

medicinal compounds with metal-specific modes of action. They have a great structural diversity (a higher number of stereoisomers and more diverse stereochemistry than the organic compounds), kinetic stability, low oxidation state of the metal centre, relative liphophilic character, redox properties of the metal cation, their ability to bind biological targets and the possibility of rational ligand design in order to control the kinetic properties, such as rate of ligand exchange. The most studied examples of organometallic species include: titanocene[40] and ferrocene[41, 42] derivatives, half-sandwich compounds of ruthenium, osmium, rhodium and iridium[8, 38, 39, 41, 43], metal carbonyl complexes[44], carbene derivatives of gold, platinum, copper, ruthenium and rhodium[15, 38, 39, 45-48] and cyclometalated complexes of gold, ruthenium, rhodium and platinum[14, 19, 38, 45, 49].

The choice of the ligand in the synthesis of an organometallic complex is of great relevance for their stability in solution. Thus, gold (III) derivatives, which can be certainly reduced in physiological conditions, can improve their stability with chelating ligands of the type C,N- or C,N,N- ligands affording cyclometalated compounds[14, 38]. Organometallics gold (I) derivatives can be easily stabilised by coordination of carbenes and alkyne ligands. As stated above, there is a huge number of gold(I) carbenes with antitumor activity described in the literature, however alkyne gold(I) complexes with potential anticancer behaviour are much less represented[50-55].

Working in this frame, we have recently described alkyne gold(I) derivatives with the ligand S-propargylthiopiridine, which display high cytotoxic activity against colon cancer[56]. Considering our previous studies in the chemistry of gold(I) derivatives with the water soluble phosphanes PTA (1,3,5-triaza-7-phosphaadamantane) and DAPTA (3,7-diacetyl-1,3,7-triaza-5-phosphabicyclo[3.3.1]nonane) as anticancer agents[57-60], we present here an extension of these previous results on additional alkyne ligands, which include the *in vitro* and *in vivo* studies and the interaction of these complexes with proteins, such as bovine serum albumin (BSA).

Results and Discussion

Synthesis and characterization

The preparation of the alkyne ligands ($RCH_2C{\equiv}CH$) (R = Spyridine, **1**; Spyrimidine, **2**; S(Me)pyrimidine, **3**; $S(Me)_2$pyrimidine, **4**) was performed by the reaction of propargyl bromide with the corresponding thiol, in the presence of a base in acetone, as previously described in the case of 2-thiolpyridine (**1**)[61]. Alkynes **1** and **3** are isolated as highly dense oils, while **2** and **4** are isolated as solids, which were purified by recrystallization. These alkynes react with [AuCl(L)] (L = PTA or DAPTA) in basic medium (KOH in methanol) to afford the air- stable alkyne gold(I) complexes [$Au(C{\equiv}CCH_2R)$] (R = Spyridine, L = PTA, **5**, DAPTA, **6**; Spyrimidine, L = PTA, **7**, DAPTA, **8**; S(Me)pyrimidine, L = PTA, **9**, DAPTA, **10**; $S(Me)_2$pyrimidine, L = PTA, **11,** DAPTA, **12**) (Scheme 1).

All the complexes show singlet resonances in their $^{31}P\{^1H\}$ NMR spectra at about -50 ppm for PTA derivatives and around -20 ppm for DAPTA complexes, downfield displaced with respect to that for the starting chloro gold(I) compounds. The absence of the alkyne resonance observed at around 2.7 ppm in the ^{1}HNMR spectra in the free ligands confirms the metallic coordination trough the C≡C unit. Additionally, a slight high field displacement in the signals due to the thiolate unit is observed in the ^{1}H NMR spectra and a low field shift in the resonance of the SCH_2 group, also detected in their $^{13}C\{^1H\}$ NMR experiments, in comparison to those measured in the free ligands.

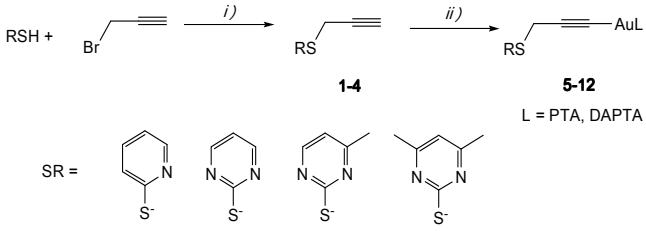

Scheme 1. (*i*) K_2CO_3, (*ii*) [AuClL]/KOMe

All the complexes display low water-solubility with values below 5 mg/mL at room temperature, except compound **5**, with a water solubility of 82 mg/mL. Nevertheless, they are regularly distributed between water and n-octanol, as deduced by the values observed in their corresponding partition coefficients (log $D_{7.4}$) next to 0 (Table 1). There is a good agreement with these values and the water-solubility. Thus, the most water soluble derivatives show negative coefficients and consequently [$Au(C{\equiv}CCH_2SMepyrimidine)(PTA)$] (**9**), with a log $D_{7.4}$ of +0.72, is the least water-soluble complex. There are no differences between both phosphanes PTA and DAPTA, in fact a similar behaviour is observed in couples using the same propargylthiol unit. $C{\equiv}CCH_2$Spyridine and $C{\equiv}CCH_2SMe_2$pyrimidine give the best relationship between lipophilic and hydrophilic character, with values essentially 0.

Biological studies

The cytotoxic effects of these propargylthiol derivatives have been tested against human colon cancer cell lines, clones Caco-2/PD7 and Caco-2/TC7 (isolated from early and late passage respectively). Both clones were selected on basis of differences in the levels of expression of the enzyme sucrase-isomaltase (SI) in the brush border of the small intestine and rates of glucose consumption[62].

View Article Online
DOI: 10.1039/C5DT01802A

Table 1 resumes the IC_{50} values obtained after 72h of exposure to the drug in comparison to cisplatin and auranofin, using the MTT assay (see experimental section). In general, all the complexes are cytotoxic to both clones and display considerably higher cytotoxicity than that observed with cisplatin. Similar or higher IC_{50} values are obtained in comparison with auranofin, and in the same order than those previously reported for related gold derivatives described by us[50, 56]. Notably, the derivatives with the phosphane PTA are more effective than their partners with DAPTA, with slight differences between them and between clones, giving mostly higher IC50 values for the TC7 clone. Hardly any influence of the substituent in the thiolate unit can be inferred from these experimental data, since similar IC50 values are recorded in the PTA complexes (values ranging from 2.6 to 3.6 μM in Caco-2/PD7 and from 2.7 to 4.5 μM in Caco-2/TC7 cell line). However, slightly higher differences are detected in the DAPTA partners and the presence of two methyl groups in the thiolate moiety increase moderately the activity (see complex **12**) in the DAPTA family. There is no relationship between the liphophilic and hydrophilic character and anticancer activity. Thus, the most active compounds, the ones with the PTA molecule, display log$D_{7.4}$ values next to 0, except in [Au(C≡CCH_2SMepyrimidine)(PTA)] (**9**) with higher lipophilic character (log$D_{7.4}$ = +0.72).

Table 1. IC_{50} values of metallic complexes against PD7 and TC7 colon cancer cell lines compared with auranofin and cisplatin

		IC_{50} (μM)[a]	
Compound	**log$D_{7.4}$**	**PD7**	**TC7**
[Au(C≡CCH_2Spyridine)(PTA)] (**5**)	–0.07	3.6 ± 0.3	4.5 ± 0.2
[Au(C≡CCH_2Spyridine)(DAPTA)] (**6**)	–0.03	13.1 ± 1.6	14.9 ± 0.7
[Au(C≡CCH_2Spyrimidine)(PTA)] (**7**)	–0.15	2.7 ± 0.4	2.7 ± 0.1
[Au(C≡CCH_2Spyrimidine)(DAPTA)] (**8**)	–0.16	14.4 ± 2.1	9.3 ± 1.9
[Au(C≡CCH_2SMepyrimidine)(PTA)] (**9**)	+0.72	2.8 ± 1.5	2.7 ± 0.26
[Au(C≡CCH_2SMepyrimidine)(DAPTA)] (**10**)	+0.27	9.9 ± 4.1	8.9 ± 2.2
[Au(C≡CCH_2SMe_2pyrimidine)(PTA)] (**11**)	+0.01	2.6 ± 1.9	3.7 ± 0.2
[Au(C≡CCH_2SMe_2pyrimidine)(DAPTA)] (**12**)	+0.04	4.2 ± 2.8	8.0 ± 2.1
Cisplatin		37.2 ± 5.1	45.6 ± 8.1
Auranofin		1.8 ± 0.1	2.1 ± 0.4

[a] Mean ± SE of at least three determinations

Interaction of the metallic complexes with BSA

Considering that most of the anticancer drugs are intravenously administrated, the study of their possible interaction with blood components is of general interest. The interaction with serum proteins can determine the overall drug distribution and excretion and differences in efficacy, activity and toxicity[63]. In general, the metabolism of a drug can be significantly altered by its binding to the serum protein[64]. Bovine serum albumin (BSA) is one of the most studied proteins due to its similar structure to human serum albumin (HSA)[65]. It is the most abundant protein in blood plasma and principle extracellular source of sulfhydryl groups in the circulatory system; it transports different substrates, including metals, amino acids, hormones, fatty acids and medicinal drugs. BSA comprises of a chain of 580 amino acids residues with a well-known structure consisting of a single peptide chain that contains two tryptophans, Trp-134 and Trp-212, which possess intrinsic fluorescence[66]. Trp is highly sensitive to its local environment, being possible to observe changes in the fluorescence emission spectra in cases of protein conformational changes or binding to substrates. The quenching of the BSA fluorescence is a powerful method to study substrates interactions and/or binding to the protein, thanks to its high sensibility and quick response. Thus, several examples of fluorescence quenching studies *via* metallic interaction with the protein serum albumin can be found in the literature, including examples of gold nanoparticles[67-70]

In order to confirm the interaction between BSA and the metallic derivatives and to obtain a quantitative binding constant, we have measured the fluorescence of the BSA in the range of 310-450nm upon excitation at 295nm and in the presence of varying concentrations of complexes **5-12** (see experimental for details).

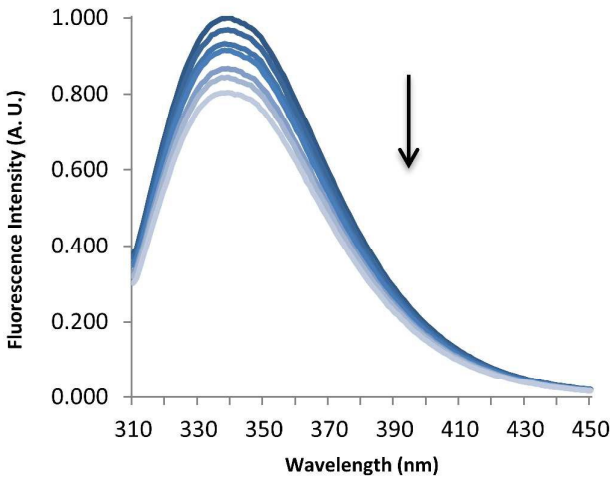

Figure 1. Fluorescence quenching spectra of BSA at different concentrations of **5** at 298 K.

Before the analysis, we measured the luminescence of the gold (I) derivatives and under our experimental conditions, no fluorescence emission in the range of 295-500 nm was observed for them. The complexes display a decrease in the intensity of the fluorescence signal as a function of increasing concentration, without changes in the emission maximum or in their shape (figure 1). This quenching of the fluorescence implies that the microenvironment around the

View Article Online
DOI: 10.1039/C5DT01802A

chromophore of BSA is changed upon addition of the metallic complexes.

The values obtained in these complexes for the binding constant to serum albumin are in the range of 10^1 to 10^3 (Table 2). These values

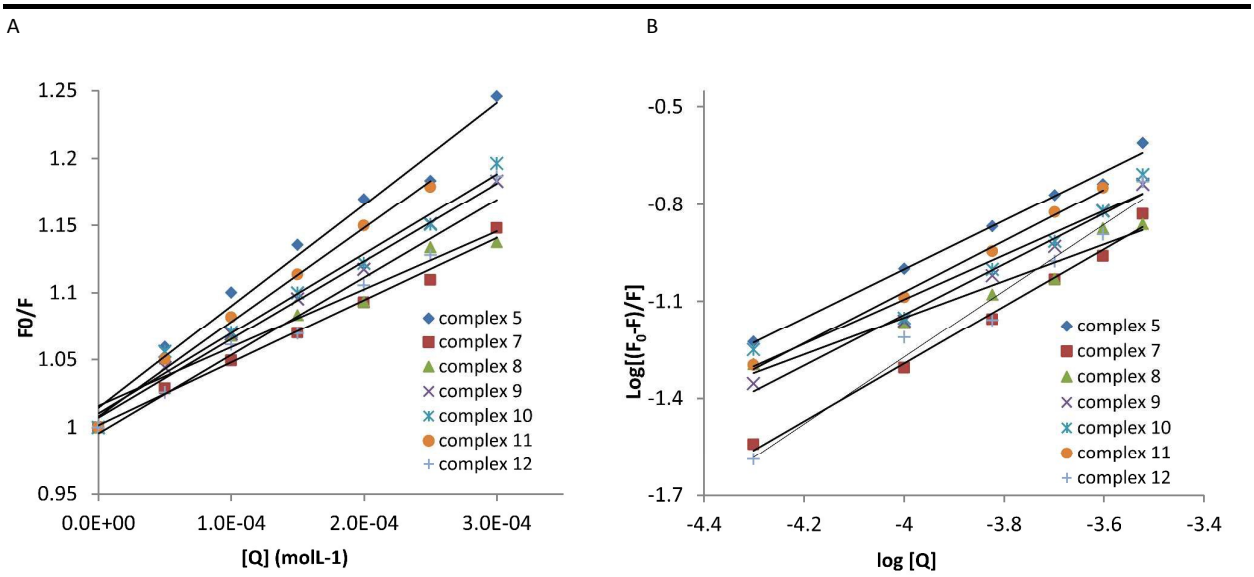

Figure 2. (A) Stern-Volmer plot for the quenching of BSA with complexes **5-12**. Stern-Volmer equation used: $F_0/F = 1 + K_{sv}[Q]$. The slope of the best fit linear trend provides the Stern-Volmer quenching constant K_{sv}. (B) Stern-Volmer plot for the quenching of BSA with complexes **5-12**. Stern-Volmer equation used: $\log\{(F_0-F)/F\} = \log K_b + n\log[Q]$. The intercept of the best fit linear trend provides the Stern-Volmer quenching constant K_b.

Fluorescence intensity data were analysed according to Stern-Volmer quenching equation $F_0/F = 1 + K_{sv}[Q] = 1 + K_q\tau_0[Q]$, where F_0 and F are the steady state fluorescence intensities of BSA before and after complex addition, K_{sv} is the Stern-Volmer dynamic quenching constant, K_q is the quenching rate constant, τ_0 is the quenching constant (average lifetime without the quencher) and [Q] is the concentration of the quencher complex. The plot of (F_0/F) *vs.* [Q] (figure 2A) provides K_{sv} and using the standard value of 10^{-8}s for τ_0 is possible to calculate the corresponding values for the quenching rate constant K_q (Table 2).

When small molecules bind to a set of equivalent sites on a macromolecule, the equilibrium between free and bound molecules can be given by the modified form of the Stern-Volmer equation (double logarithm regression curve: $\log\{(F_0-F)/F\} = \log K_b + n\log[Q]$). This equation can be used to determine the binding constant (K_b) or the apparent association constant for complex-protein interaction and the number of binding sites (n). Both parameters can be deduced from the intercept and slope, respectively, by plotting $\log\{(F_0-F)/F\}$ versus log[Q] (figure 2B).

Table 2. Values of Stern-Volmer quenching constant (K_{sv}), quenching rate constant (K_q) and apparent binding constant (K_b) for the interaction of complexes **5-12** with BSA

Complex	K_{sv} (L mol^{-1})	K_q (L mol^{-1} s^{-1})	K_b (M^{-1})
[Au(C≡CCH$_2$Spyridine)(PTA)] (**5**)	7.54 10^3	7.54 10^{11}	6.04 10^2
[Au(C≡CCH$_2$Spyrimidine)(PTA)] (**7**)	4.64 10^3	4.64 10^{11}	1.40 10^3
[Au(C≡CCH$_2$Spyrimidine)(DAPTA)] (**8**)	4.32 10^3	4.32 10^{11}	5.00 10^1
[Au(C≡CCH$_2$SMepyrimidine)(PTA)] (**9**)	5.80 10^3	5.80 10^{11}	6.11 10^2
[Au(C≡CCH$_2$SMepyrimidine)(DAPTA)] (**10**)	5.93 10^3	5.93 10^{11}	2.23 10^2
[Au(C≡CCH$_2$SMe$_2$pyrimidine)(PTA)] (**11**)	7.00 10^3	7.00 10^{11}	7.86 10^2
[Au(C≡CCH$_2$SMe$_2$pyrimidine)(DAPTA)] (**12**)	5.78 10^3	5.78 10^{11}	5.78 10^3

are next to the observed in cisplatin, with a K_b of 8.52 10^2 M^{-1} with a human serum albumin[71]. Higher values around 10^4-10^5 M^{-1} are found in gold (III) derivatives[68, 72] and in the dicyano gold(I) complex $[Au(CN)_2]^-$ [73] and about 10^{10} in the case of gold nanoparticles[70], which are in accordance with stronger interaction of the reported derivatives with the protein. Values below 1 in n (ranging from 0.6 to 1) are indicative that there is approximately one class of binding site for the gold complexes towards BSA. Binding to serum albumin is important for selective drug delivery. However, if the interaction is too strong, the drug might not be released to the target. The moderate values of binding constants in our complexes could indicate that they can be stored and carried by this protein in the body and be easily released.

View Article Online
DOI: 10.1039/C5DT01802A

Table 3. Values of quenching constant (*Ksv*), apparent binding constant (*Kb*) and thermodynamic parameters for BSA-**5** system at different temperatures.

T (K)	K_{SV} (L mol^{-1})	K_b (L mol^{-1})	R^2	ΔH^o (KJ mol^{-1})	ΔG^o (KJ mol^{-1})	ΔS^o (J mol^{-1}K^{-1})
292	7.98 10^3	2.34 10^4	0.9894	-181.28	-18.94	-555.96
298	7.54 10^3	6.04 10^2	0.9905		-15.61	
304	7.47 10^3	1.22 10^2	0.9626		-12.27	

A linear Stern-Volmer plot (figure 2A) is indicative of a single quenching mechanism, either dynamic or static[74]. We examined the effect of temperature on the interaction of one of the complexes, in the particular case of complex **5,** to BSA, in order to distinguish both mechanisms. Dynamic or collisional quenching depends upon diffusion, since higher temperatures give higher diffusion coefficients, consequently the quenching constants increase with increasing temperatures[75]. A static quenching process involves the formation of a non-fluorescent ground state complex between the fluorophore and the quencher and the quenching constants decrease with increasing temperatures[74]. In our case, we observed that K_{sv} for complex **5** (table 3) was inversely correlated with temperature, which is indicative of a static quenching rather than dynamic collision. In addition, the values of the binding constants K_b decreased with the temperature, which may indicate the formation of a less stable compound. The decreasing tendency of K_b with increasing temperature is in accordance with K_{sv} dependence on the temperature, shown in Table 3.

The interaction forces between small molecules and biomolecules include hydrogen bonds, van der Waals forces, electrostatic and hydrophobic attraction. The sign of the thermodynamic parameters ΔG^o, ΔH^o and ΔS^o of the reaction are important for the study of the interaction forces[76]. Thus, values of $\Delta H^o > 0$ and $\Delta S^o > 0$ are indicative of hydrophobic interactions, $\Delta H^o < 0$ and $\Delta S^o < 0$ by hydrogen bonding or van der Waals interactions and $\Delta H^o \sim 0$ and $\Delta S^o > 0$ by electrostatic interactions. The corresponding thermodynamic parameters for the interaction between complex **5** and BSA were calculated from the van´t Hoff equation: $\ln K_b = -\Delta H^o/RT + \Delta S^o/R$, where K_b is the binding constant calculated at different temperatures and R is the gas constant. The enthalpy exchange ΔH^o is calculated from the slope of the plot of $\ln K_b$ *vs*. 1/T (figure S17, supporting information) and the free energy change ΔG^o is estimated from the relationship $\Delta G^o = \Delta H^o - T\Delta S^o$. According to the data recorded in Table 3 the negative values for ΔH^o and ΔS^o indicate van der Waals interactions or hydrogen bonding, and $\Delta G^o < 0$ supports the presence of a spontaneous process.

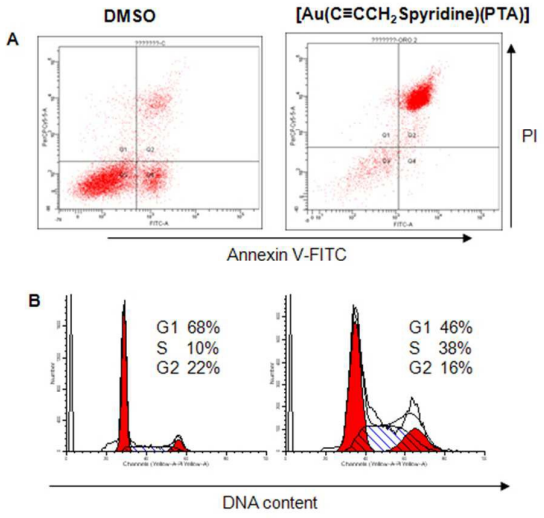

Figure 3. (A) Cell cycle distribution of HCT-116-luc2 colon cancer cells treated with 20μM of [Au(C≡CCH$_2$Spyridine)(PTA)] (**5**) for 72 h. (B) Quantitative flow cytometry analyses using propidium iodide (PI) uptake and annexin V staining in HTC-116 cells treated with DMSO and 20μM in gold complex after 72h.

Table 4. Cell uptake of gold complexes in Caco-2/PD7 cells after treatment with 1μM gold compounds

Complex	*pmol/10^6 cells*
[Au(C≡CCH$_2$Spyridine)(PTA)] (**5**)	2368.9
[Au(C≡CCH$_2$Spyrimidine)(PTA)] (**7**)	3272.1
[Au(C≡CCH$_2$Spyrimidine)(DAPTA)] (**8**)	163.3

Solution stability study.

The stability in solution of the different complexes has been checked by study of their UV-Vis spectra recorded every two hours, under physiological conditions. No visible changes (colour, turbidity, decomposition to metallic gold, etc.) could be observed, with exception of complex **11** which precipitated as soon as it was diluted in the PBS medium, due to its poor solubility. All the complexes display some relevant time-dependent spectral changes as the decrease of a band at about 250nm and the appearance of a new one in the range 320-330 nm, that may be ascribed, quite straightforward, to progressive aquation of the alkyne derivative, similarly to previously observed in other described gold(III) derivatives.[77]The changes observed in these spectra, point out that these complexes undergo progressive transformations in the physiological medium that imply that they are acting as pro-drugs.

Cell uptake studies.

We have measured the cell uptake of three of the complexes here described after incubation of 1μM solutions of complexes **5**, **7** and **8** with Caco-2/PD7 cells for 3h at 37ºC followed by ICP-MS analysis, as described in experimental section. The results expressed as pmol Au/mg protein are recorded in Table 4. Accordingly with the IC_{50} values recorded in Table 1, the most active derivatives **5** and **7**, display the highest uptake values, however a lower value is measured for the DAPTA partner [Au(C≡CCH$_2$Spyrimidine)(DAPTA)] (**8**), that fits well with its lower IC_{50} value, probably due to a worse permeability of the DAPTA ligand compared to the PTA. The obtained values are in agreement to what some of us previously observed for Au(I) thiolate complexes entering ovarian cancer cells.[59]

View Article Online
DOI: 10.1039/C5DT01802A

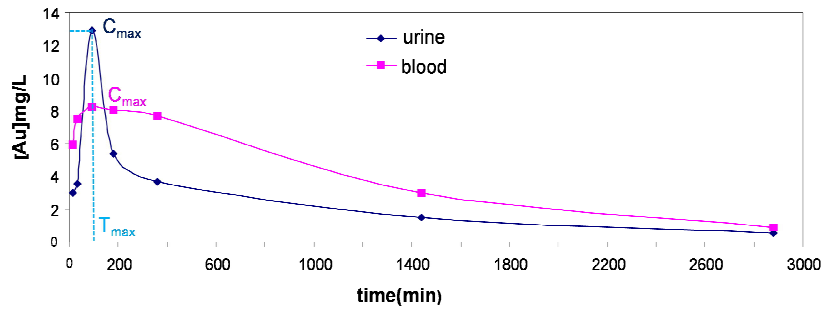

Figure 4. Gold concentration in urine (blue) and in blood (pink) as a function of time after intraperitoneal injection of 5 mg/kg of [Au(C≡CCH$_2$Spyridine)(PTA)] (**5**) in mice. C_{max} is the maximal concentration achieved; T_{max} is the time take to achieve the maximal concentration.

***In vivo* experiments**

The promising *in vitro* results obtained for colon cancer cell lines encouraged us to test their ability to inhibit tumour growth *in vivo* by using xenograft tumours in nude mice. We chose [Au(C≡CCH$_2$Spyridine)(PTA)] (**5**) due to its low and homogeneous IC_{50} values obtained in both cancer cell lines, the intermediate value of binding constant of the derivatives and the highest water solubility value measured from all the complexes tested *in vitro*.

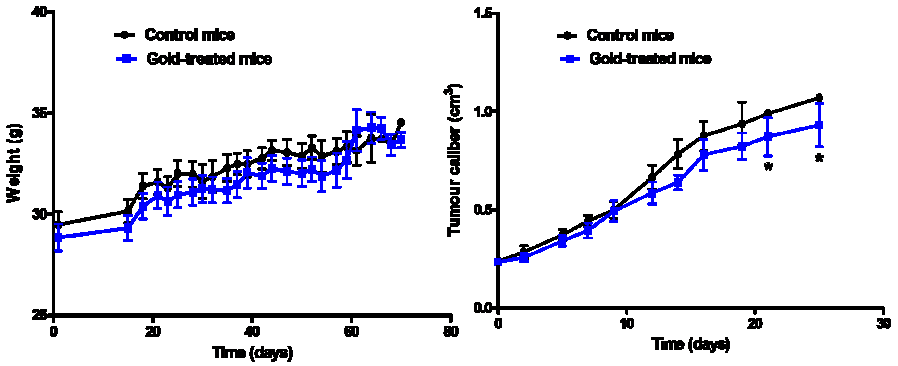

Figure 5. (A) Changes of body weight against number of days of mice treated with [Au(C≡CCH$_2$Spyridine)(PTA)] (**5**) in comparison with control mice. Results are shown as mean ± standard deviation (N = 6 mice). (B) Results showing the changes of HCT-116-luc2 tumour volume (measured with calliper) against time in mice treated with complex **5** in comparison with control mice. *P < 0.05 *vs*. control.

To evaluate the effect of the gold derivative on tumour growth, HCT-116 cells overexpressing luciferase (HCT-116-luc2) were injected subcutaneously into immune deficient mice. Prior to the injection, we achieved the *in vitro* test of complex **5** with the HCT-116-luc2 cells by using the well-established MTT assay. As expected, a higher IC_{50} value (6.09 ± 0.27 *vs.* 3.65 ± 0.34 or 4.53 ± 0.18 in Caco-2 cell lines) was obtained, owing to the greater aggressiveness of the HCT-116-luc2 cells.

As occurred in the Caco-2/PD7 and TC7 cell lines[56], flow cytometry displayed cell death induction by apoptosis after incubation of [Au(C≡CCH$_2$Spyridine)(PTA)] (**5**) with HCT-116-luc2 cancer cells. Thus, figure 3A shows that only 8% of living cells remain after 72 hours of gold-treatment and only apoptotic cells (1.9 % in early-stage apoptosis and 89.3% in late-stage apoptosis) can be detected.

One of the aims of cancer chemotherapy is to attack the malignant cells during one or more phases of its reproductive cycle. There is considerable evidence that the DNA damaging agents such as cisplatin and related platinum-based drugs, for instance oxaliplatin, (mainly used in the treatment of metastatic colorectal carcinoma) alter the cell cycle progression. Thus, cancer cells treated with these chemotherapeutic agents display arrest in G2/M phase of the cell cycle inhibiting the cell division[78, 79]. In our case the analysis of the DNA content of cells stained with propidium iodide by flow cytometry shows an increase of the cellular population in the S-phase with a concomitant decrease in the G1-phase (46% *vs*. 68% in DMSO) (figure 3B) involving an S-phase arrest, the period of the DNA synthesis[80].

For a compound not given directly into the bloodstream by intravenous administration, it is necessary to be transported from the site of administration into the systemic circulation. Apart from the factors affecting the drug transport across the membranes, its absorption depends on a number of physicochemical factors, the two most important of which are lipophilicity and water-solubility[81]. For this reason, it is of considerably interest the use of derivatives with a balanced relationship between lipophilicity and hydrophilicity. As stated in table 1, most of the propargyl phosphane complexes display values of log$D_{7.4}$ next to 0, consequently they are good candidates for the *in vivo* text. Since our gold complex tested *in vivo* is administrated *via* intraperitoneal injection, it is important to determine the corresponding Cmax (maximal concentration achieved after intraperitoneal injection) and Tmax (the time lapsed to achieve such maximal concentration) both in blood and in urine. Thus, the concentration of gold in the blood and urine of the treated mice was determined by ICP-MS after intraperitoneal administration of 5 mg/kg body weight (bw) of [Au(C≡CCH$_2$Spyridine)(PTA)] (**5**) to CD1 mice weighing between 18

View Article Online
DOI: 10.1039/C5DT01802A

and 20 g were 8.26 ng/μL in blood and 12.91 ng/μL in urine at 90 min. As it can be seen in figure 4, the maximal concentration in blood is practically maintained during the following 5 hours, decreasing gradually up to a value of 0.9 ng/μL at 48 hours. At this time, the concentration in urine reached a value of 0.58 ng/μL.

We investigated the *in vivo* effect of complex **5** on established subcutaneous tumours. Thus, athymic nude mice xenografted with human HCT-116-luc2 cancer cells were employed to evaluate the *in vivo* antitumor activity. Twelve male mice were randomly divided into a control group (treated with vehicle, DMSO) and a group treated with 5 mg/kg -bw- of [Au(C≡CCH$_2$Spyridine)(PTA)] (**5**) three times per week on alternative days to a tumour volume of 1 cm^3. No significant weight changes were observed in either group during treatment. Indeed, Figure 5A shows an overall increase in body weight, similar in both groups of mice.

Figure 5B shows the differences in tumour volume measured with a calliper. It was observed during the experiment that the average tumour volume for the gold treated mice display a more slowly increase in comparison to the control mice and show a statistically substantial difference. Moreover, a significant decrease in the bioluminescence signal is observed during the last days of the study (figure 6), which is in accordance with a decrease in the number of malignant cells after gold treatment. In addition, figure 7 shows the survival curve for thirty-one days. As can be seen from the figure, a higher percentage of survival is observed in gold-treated mice, since all mice in this group survived up to day 16 (day 12 for the control group) and the last death took place around the day 31 (*vs.* 21 in the control mice). Additionally, an increase in the mean survival time (MST) is achieved, with MST of 16.5 days in mice transplanted with vehicle (control mice) and 23.5 days in gold-treated mice. Besides, the increase in the life span (ILS) of tumour-bearing mice upon treatment with the gold complex was found to be 42.7% with respect to the control group.

Reduction in tumour growth was also observed in previous *in vivo* studies[82-84] in mice inoculated with HCT-116 colon cancer after treatment with platinum derivatives, such as cisplatin or oxaliplatin. Ii has been also observed that the adminsitration of brostallicilin or curcumin as coadjuvants, enhances the corresponding platinum drug's efficacy[82, 83].

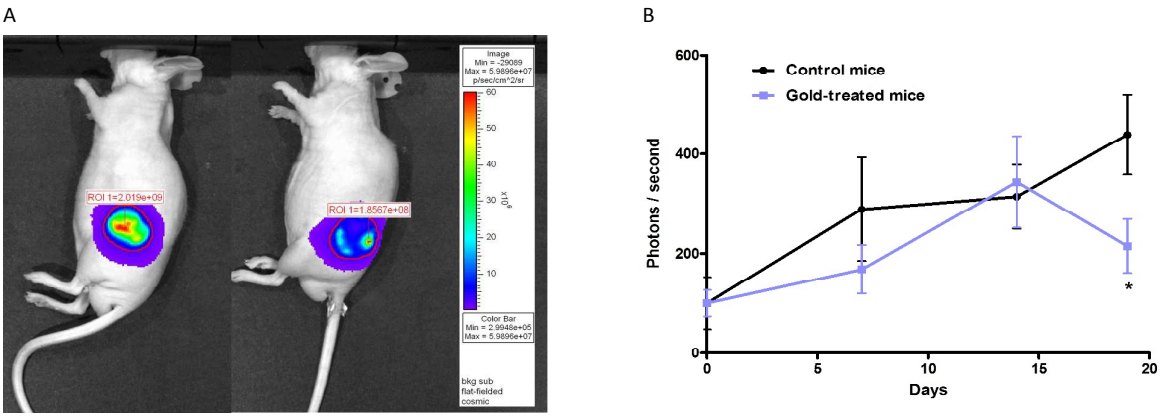

Figure 6. (A) Bioluminescence images after injection of luciferin to mice infected with HCT-116-luc2. (B) Results showing the changes of HCT-116-luc2 tumour volume against number of days in mice treated with [Au(C≡CCH$_2$Spyridine)(PTA)] (**5**) in in comparison with control mice. *P < 0.05 *vs*. control

At the end of the observation period, the dead or sacrificed mice were dissected and subjected to a histological assessment of organ damage. We observed similar histological findings for the kidney, liver and tumour in control and in treated mice (Figures 8-10), which implies that this gold derivative does not exert any undesirable effects in mice *per se*. Similar results have been achieved recently in the thiolate gold (I) PTA derivative [Au(Spyrimidine)(PTA-CH$_2$Ph)]Br[85].

Experimental

General procedures

NMR Spectroscopy. ^{1}H, ^{31}P and ^{13}C NMR spectra were recorded on 400 or 300 MHz Bruker Avance spectrometers and are referenced to external TMS or 85% H_3PO_4 (^{31}P), Chemical shifts (δ) are given in ppm, coupling constants are reported in Hz. MALDI mass spectra were measured on a Micromass Autospec spectrometer in positive ion mode using DCTB (1,1-diciano-4-^{t}butylphenyl-3-methylbutadiene) or DIT (dithranol) as matrix. HRMS were measured on a Bruker MicroTof-Q spectrometer. Infrared spectra (4000-250cm^{-1}) were recorded on a Perkin Elmer Spectrum 100 FTIR (far-IR) spectrometer. Elemental analyses were obtained in-house using a LECO CHNS-932 microanalyser. The starting material: the phosphanes PTA[86] and DAPTA[87], HC≡CCH$_2$Spyridine[61], [Au(C≡CCH$_2$Spyridine)L] (L = PTA, **5** and DAPTA, **6**)[56] and *auranofin*[88] were prepared according to published methods. *Cisplatin* was purchased from Sigma-Aldrich.

View Article Online
DOI: 10.1039/C5DT01802A

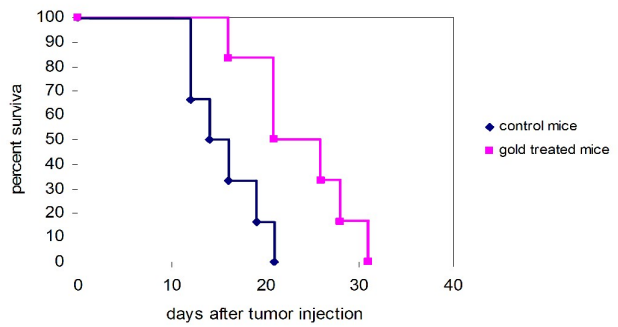

Figure 7. Survival data plotted as percent of animals surviving in each group using a predefined cut-off volume of 1.000 mm^3 as a surrogate for survival

Synthesis

Preparation of the propargylthiopyrimidines. K_2CO_3 in excess and propargylbromide (1.6 equivalents) were added to a solution of pyrimidine-2-thiol, 4-methylpyrimidine-2-thiol or 4,6-dimethylpyrimidine-2-thiol. The reaction was heated under reflux for 8 hours, and after this time, the excess of base was filtered off and the residue was evaporated to dryness.

2-Propargylthiopyrimidine (2). Yield: 61% red solid. ^{1}H NMR (400 MHz, acetone-d^6) δ(ppm) = 8.63 (d, 2H, *J* = 4.9 Hz, *H*^{4} and *H*^{6}), 7.22 (t, 1H, J = 4.9 Hz, *H*^{5}), 3.98 (d, 2H, J = 2.7 Hz, SCH_2), 2.66 (t, 1H, J = 2.6 Hz, C≡C*H*); ^{13}C{^{1}H}NMR (101 MHz, acetone-d^6) δ = 171.2 (s, 1C, Ph), 158.6 (s, 2C, *C*^{4} and *C*^{6}), 118.2 (s, 1C, *C*^{5}), 72.1 (s, 1C, *C*≡CH), 19.4 (s, 1C, S*C*H$_2$). HRMS: found [M+H]$^+$ 151.0329, $C_7H_7N_2S$ requires 151.0328.

2-Propargylthio-4-methylpyrimidine (3). Yield: 80% purple oil. ^{1}H NMR (400 MHz, acetone-d^6) δ(ppm) = 8.37 (d, 1H, *J* = 5.1 Hz, *H*^{6}), 6.83 (d, 1H, *J* = 5.1 Hz, *H*^{5}), 3.91 (d, 2H, *J* = 2.6 Hz, SCH_2), 2.40 (s, 3H, *Me*), 2.15 (t, 1H, *J* = 2.6 Hz, C≡C*H*). ^{13}C{^{1}H}NMR (101 MHz, acetone-d^6) δ = 169.2 (s, 1C, *C*^{4}), 158.4 (s, 1C, *C*^{6}), 117.9 (s, 1C, *C*^{5}), 72.4 (s, 1C, C≡CH), 24.3 (s, 1C, *Me*), 19.4 (s, 1C, S*C*H$_2$).

2-Propargylthio-4,6-dimethylpyrimidine (4). Yield: 84% pink solid. ^{1}H NMR (400 MHz, acetone-d^6) δ(ppm) = 6.94 (s, 1H, *H*^{5}), 3.97 (d, 2H, *J* = 2.7 Hz, SCH_2), 2.65 (t, 1H, *J* = 2.7 Hz, C≡C*H*), 2.38 (s, 6H, *Me*), ^{13}C{^{1}H}NMR (101 MHz, acetone-d^6) δ = 168.3 (s, 2C, *C*^{4} and *C*^{6}), 116.8 (s, 1C, *C*^{5}), 71.9 (s, 1C, C≡CH), 23.7 (s, 2C, *Me*), 19.2 (s, 1C, S*C*H$_2$). HRMS: found [M+H]$^+$ 179.0647, $C_8H_{11}N_2S$ requires 179.0637.

Synthesis of the [Au(C≡CCH$_2$SR)L] complexes. To a solution of KOH (0.014 g, 0.25 mmol) in MeOH (ca. 10 mL) containing the 2-propargylthiopirimidine (0.2 mmol) [AuCl(L)] (L = PTA, DAPTA) (0.2 mmol) was added. The corresponding solids precipitated in the methanolic solution, and were isolated by filtration after 20 h of stirring at room temperature, washed with methanol and diethyl ether, and dried in *vacuo*. Using this method the following complexes were prepared:

[Au(C≡CCH$_2$Spyrimidine)PTA] (7). Yield: 80% yellow solid. ^{1}H NMR (400 MHz, $CDCl_3$, 25 °C) δ(ppm) = 8.49 (d, 2H, *J* = 4.8 Hz, *H*^{4} and *H*^{6}), 6.92 (t, 1H, *J* = 4.8 Hz, *H*^{5}), 4.54 and 4.42 (AB system, 6H, J_{AB}= 16.00 Hz, NC*H*$_2$N), 4.22 (s, 6H, PC*H*$_2$N), 4.06 (s, 2H, S*C*H$_2$); ^{31}P {^{1}*H*} NMR (162 MHz, $CDCl_3$) δ(ppm): −50.8 (s). ^{13}C{^{1}H} NMR (100MHz, $CDCl_3$): δ = 157.4 (s, *C*^{4}, *C*^{6}), 119.4 (s, *C*^{5}), 73.4 (d, *J* = 7.3 Hz, NC*H*$_2$N), 52.6 (d, *J* = 20.2 Hz, PC*H*$_2$N), 21.2 (s, S*C*H$_2$). IR (KBr): 2128 cm^{-1} ν(C≡C). MALDI MS: *m/z* (%): 504.12 (100) [*M+H*]$^+$, 857.14 (43) [*M+AuPTA*]$^+$. Elemental analysis calcd. (%) for $C_{13}H_{17}AuN_5PS$ (503.06): C 31.02, H 3.40, N 13.91, S 6.37; found: C 30.56, H 3.39, N 13.44, S 6.57.

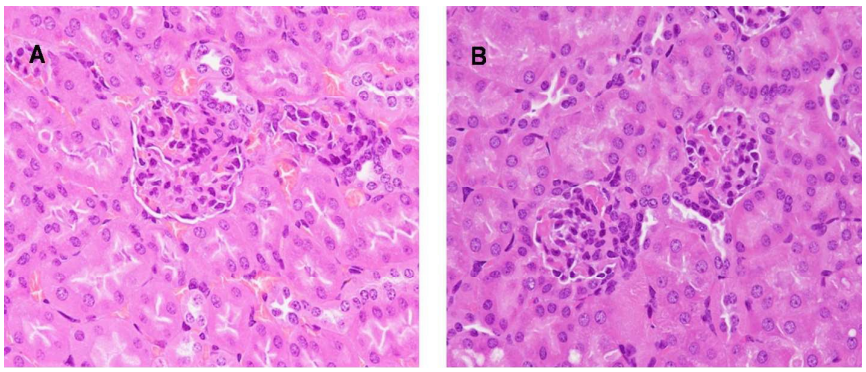

Figure 8. Histological section of a kidney from a control mouse (A) and a mouse treated with [Au(C≡CCH$_2$Spyridine)(PTA)] (**5**) (B). Both kidneys show similar characteristics with slight hypercellularity in the glomeruli and normal proximal convoluted tubules H. & E. X 400.

[Au(C≡CCH$_2$Spyrimidine)DAPTA] (8). Yield: 73% light yellow solid. ^{1}H NMR (400 MHz, dmso-d^6) δ(ppm) = 8.63 (d, 2H, *J* = 4.8 Hz, *H*^{4} and *H*^{6}), 7.21 (t, 1H, *J* = 4.8 Hz, *H*^{5}), 5.49 (d, 1H, *J* = 13.8 Hz, NC*H*$_2$N), 5.29 (dd, 1H, *J* = 15.2, 8.4 Hz, NC*H*$_2$P), 4.88 (d, 1H, *J* = 13.8 Hz, NC*H*$_2$N), 4.78-4.72 (m, 1H, NC*H*$_2$P), 4.6 (d, 1H, *J* = 13.7 Hz, NC*H*$_2$N), 4.23-4.08 (m, 3H, 2NC*H*$_2$P+NC*H*$_2$N), 4.05 (2H, s, S*C*H$_2$), 3.64 (d, 2H, *J* = 15.8 Hz, NC*H*$_2$P), 1.95 (6H, s, $COCH_3$). ^{31}P{^{1}*H*} NMR (162 MHz, $CDCl_3$) δ(ppm): −22.4 (s). ^{13}C{^{1}H} NMR (100MHz, dmso-d^6): δ = 169.4 (s, *C*=O), 157.8 (s, *C*^{4}, *C*^{6}), 117.3 (s, *C*^{5}), 97.5 (s, *C*≡*C*), 66.5 (s, NCH$_2$N), 61.0 (s, NCH$_2$N), 47.3 (d, *J* = 25.4Hz, PCH$_2$N), 43.8 (d, *J* = 25.5Hz, PCH$_2$N), 38.3 (d, *J* = 26.5Hz, PCH$_2$N), 21.5 (s, *C*H$_3$), 20.6 (s, S*C*H$_2$). IR (KBr): 1646 ν(C=O), 2161 cm^{-1} ν(C≡C). MALDI MS: *m/z* (%): 576.13 (100) [*M+H*]$^+$, 1001.16 (5) [*M+AuDAPTA*]$^+$. Elemental analysis calcd. (%) for $C_{16}H_{21}AuN_5O_2PS$

View Article Online
DOI: 10.1039/C5DT01802A

(575.08): C 33.40, H 3.68, N 12.17, S 5.57; found: C 33.13, H 4.02, N 11.48, S 5.09

[Au(C≡CCH$_2$SMe-pyrimidine)PTA] (9). Yield 71% light yellow solid. ^{1}H NMR (400 MHz, CDCl$_3$) δ(ppm) = 8.34 (d, 1H, *J* = 5.1 Hz, *H*^{6}), 6.77 (d, 1H, *J* = 5.1 Hz, *H*^{5}), 4.51 and 4.42 (AB system, 6H, J_{AB} = 16.00 Hz, NC*H*$_2$N), 4.23 (s, 6H, PC*H*$_2$N), 4.05 (s, 2H, SC*H*$_2$), 2.41 (s, 3H, C*H*$_3$); ^{31}P{^{1}*H*} NMR (162 MHz, CDCl$_3$) δ(ppm) = –50.8 (s). ^{13}C{^{1}H} NMR (100MHz, CDCl$_3$): δ = 156.9 (s, *C*^{6}), 116.3 (s, *C*^{5}), 99.5 (s, *C*≡*C*), 73.3 (d, *J* = 7.3 Hz, NC*H*$_2$N), 52.5 (d, *J* = 20.0 Hz, PC*H*$_2$N), 24.2 (s, *C*H$_3$), 21.2 (s, S*C*H$_2$). IR (KBr): 2161 cm^{-1} ν(C≡C). MALDI MS: *m/z* (%): 518.14 (100) [*M+H*]$^+$, 871.17 (43) [*M+AuPTA*]$^+$. Elemental analysis calcd. (%) for $C_{13}H_{17}AuN_5PS$ (517.08): C 32.50, H 3.70, N 13.54, S 6.20; found: C 31.95, H 3.46, N 12.99, S 6.11.

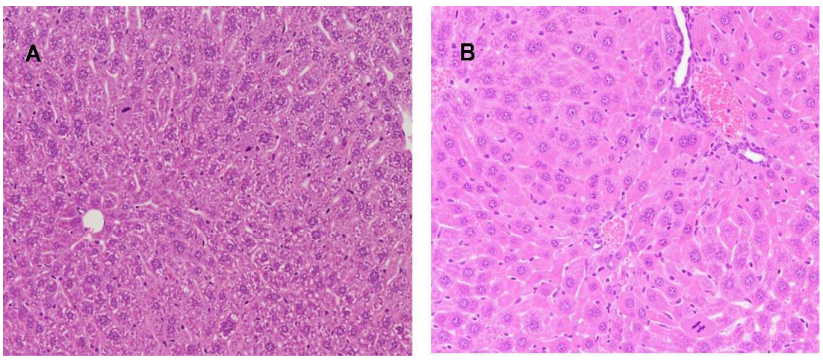

Figure 9. Section of liver histology from control mouse (A) and treated mouse with [Au(C≡CCH$_2$Spyridine)(PTA)] (**5**) (B). Normal hepatocytes, megalocytes and binucleate hepatocytes. H. & E. X 200

[Au(C≡CCH$_2$SMe-pyrimidine)DAPTA] (10). Yield 93% purple solid. ^{1}H NMR (400 MHz, CDCl$_3$) δ(ppm) = 8.28 (d, 1H, *J* = 5.1 Hz, *H*^{6}), 6.76 (d, 1H, *J* = 5.1 Hz, *H*^{5}), 5.64 (d, 1H, *J* = 14.1 Hz, NC*H*$_2$N), 5.5 (dd, 1H, *J* = 15.6, 7.3 Hz, NC*H*$_2$P), 4.82 (d, 1H, *J* = 14.1 Hz, NC*H*$_2$N), 4.7-4.62 (m, 2H, NC*H*$_2$P+NC*H*$_2$N), 4.28 (d, 1H, *J* = 15.1 Hz, NC*H*$_2$P), 4.06 (s, 1H, SC*H*$_2$) 4.0 (s, brs, 3H, 2 NC*H*$_2$P+NC*H*$_2$N), 3.68 (d, 1H, *J* = 15.9 Hz, NC*H*$_2$P), 2.37 (s, 3H, C*H*$_3$), 2.04 and 2.01 (s, 6H, COC*H*$_3$). ^{31}P{^{1}*H*} NMR (162 MHz, CDCl$_3$) δ(ppm) = –25.5 (s). ^{13}C{^{1}H} NMR (100MHz, CDCl$_3$): δ = 170.6 and 170.4 (s, *C*=O); 156.9 (s, *C*$_6$); 116.6 (s, *C*$_5$), 99.5 (s, *C*≡*C*), 67.4 (d, *J* = 4.6Hz, NCH$_2$N), 62.1 (d, *J* = 5.0Hz NCH$_2$N), 49.4 (d, *J* = 25.8Hz, PCH$_2$N), 45.1 (d, *J* = 25.2Hz, PCH$_2$N), 39.7 (d, *J* = 26.5Hz, PCH$_2$N), 24.2 (s, *C*H$_3$), 21.8 and 21.5 (s, COCH$_3$), 21.1 (s, SCH$_2$). IR (KBr): 1646 ν(C=O), 2161 cm^{-1} ν(C≡C). MALDI MS: *m/z* (%): 590.16 (100) [*M+H*]$^+$, 1015.21 (2) [*M+AuDAPTA*]$^+$. Elemental analysis calcd. (%) for $C_{16}H_{21}AuN_5O_2PS$ (586.10): C 34.64, H 3.93, N 11.88, S 5.44; found: C 34.29, H 3.83, N 11.43, S 5.49.

[Au(C≡CCH$_2$SMe$_2$-pyrimidine)PTA] (11). Yield 84% light brown solid. ^{1}H NMR (400 MHz, CDCl$_3$) δ = 6.65 (s, 1H, *Ph*^{5}), 4.55 y 4.45 (AB system, 6H, J_{AB} = 12.00 Hz, NC*H*$_2$N), 4.2 (s, 6H, PC*H*$_2$N), 4.04 (s, 2H, SC*H*$_2$), 2.36 (s, 6H, C*H*$_3$); ^{31}P{^{1}*H*} NMR (162 MHz, CDCl$_3$) δ(ppm): –51.7 (s). ^{13}C{^{1}H} NMR (100MHz, CDCl$_3$): δ = 115.7 (s, *C*^{5}), 73.4 (d, *J* = 7.2 Hz, NC*H*$_2$N); 52.6 (d, *J* = 20.3 Hz, PC*H*$_2$N), 23.9 (s, *C*H$_3$), 21.1 (s, SC*H*$_2$). IR (KBr): 2100 cm^{-1} ν(C≡C). MALDI MS: *m/z* (%): 532.16 (100) [*M+H*]$^+$, 885.18 (25) [*M+AuPTA*]$^+$. Elemental analysis calcd. (%) for $C_{15}H_{21}AuN_5PS$ (531.09): C 33.91, H 3.98, N 13.18, S 6.03; found: C 33.64, H 3.6, N 12.85, S 5.78.

[Au(C≡CCH$_2$SMe$_2$-pyrimidine)DAPTA] (12). Yield 88% White solid. ^{1}H NMR (400 MHz, CDCl$_3$) δ = 6.66 (s, 1H, *Ph*^{5}), 5.69 (d, 1H, *J* = 14.0 Hz, NC*H*$_2$N), 5.54 (dd, 1H, *J* = 16.2, 7.1 Hz, NC*H*$_2$P), 4.86 (d, 1H, *J* = 14.3 Hz, NC*H*$_2$N), 4.70-4.64 (m, 2H, NC*H*$_2$P+ NCH$_2$P), 4.28 (d, 1H, *J* = 16.9 Hz, NC*H*$_2$P), 4,13 (s, 2H, SCH$_2$), 4.07-4.0 (m, 3H, 2 NCH$_2$P+NC*H*$_2$N), 3.68 (d, 1H, *J* = 16.1Hz, NC*H*$_2$P), 2.39 (s, 6H, C*H*$_3$), 2.09 and 2.05 (s, 6H, COC*H*$_3$). ^{31}P{^{1}*H*} NMR (162 MHz, CDCl$_3$) δ(ppm): –22.5 (s). ^{13}C{^{1}H} NMR (100MHz, CDCl$_3$): δ = 170.3 and 169.8 (s, *C*=O); 116.0 (s, *C*^{5}), 99.5 (s, *C*≡*C*), 67.4 (d, *J* = 1.4Hz, NC*H*$_2$N), 62.1 (s, NC*H*$_2$N), 49.5 (d, *J* = 27.0Hz, PCH$_2$N), 45.1 (d, *J* = 24.9Hz, PCH$_2$N), 39.7 (d, *J* = 26.2Hz, PCH$_2$N), 24.0 (s, *C*H$_3$), 21.8 and 21.5 (s, CO*C*H$_3$), 20.9 (s, S*C*H$_2$). IR (KBr): 1650 ν(C=O), 2142 cm^{-1} ν(C≡C). MALDI MS: *m/z* (%): 604.16 (100) [*M+H*]$^+$, 1029.19 (16) [*M+AuDAPTA*]$^+$. Elemental analysis calcd. (%) for $C_{18}H_{25}AuN_5O_2PS$ (603.11): C 35.83, H 4.18, N 11.61, S 5.31; found: C35.42, H 3.82, N 11.14, S 5.26

Distribution coefficients (log$D_{7.4}$). The n-octanol-water coefficients of the complexes were determined as previously reported[56] using a shake-flask method. PBS buffered distilled water (100 mL, phosphate buffer [PO_4^{3-}] = 10 μM, [NaCl] = 0.15 M, pH 7.4) and n-octanol (100mL) were shaken together for 72 h to allow saturation of both phases. 1 mg of the complexes was mixed in 1 mL of aqueous and organic phase, respectively for 10 minutes. The resultant emulsion was centrifuged to separate the phases. The concentrations of the compound in each phase were determined using UV absorbance spectroscopy. Log$D_{7.4}$ was defined as log[compound$_{(organic)}$]/[compound$_{(aqueous)}$].

Solution chemistry. The stability of the gold complexes has been analysed by absorption UV spectroscopy. UV-Vis absorption spectra of the complexes were recorded on a Thermo Scientific spectrophotometer. Solutions of **5-12** (5 10^{-5}M) in Phosphate buffer (pH = 7.4) were prepared from 20 mM DMSO solutions of the complexes and thereafter monitored measuring the electronic spectra over 24 h at 37ºC.

Cellular studies

Antiproliferative assays. Caco-2 cell line PD7 and TC7 clones were kindly provided by Dr. Edith Brot-Laroche (Université Pierre et Marie Curie-Paris 6, UMR S 872, Les Cordeliers (France), HCT-116-luc2 cells were provided by Perkin Elmer (Reference 124318). All the cells were maintained in a humidified atmosphere of 5% CO_2 at

View Article Online
DOI: 10.1039/C5DT01802A

37ºC. Caco-2 cells (passages 50-80) were grown in Dulbecco's Modified Eagles medium (DMEM) (Gibco Invitrogen, Paisley, UK) supplemented with 20% foetal bovine serum (FBS), 1% non-essential amino acids, 0.5 % penicillin (1000 U/ml), 0.5 % streptomycin (1000 μg/ml) and 1% amphotericin (250 U/ml). HCT-116 cells were grown in McCoy's 5A modified medium (ATCC 30-2007) supplemented with heat-inactivated FBS at a final concentration of 10% along with 1% penicillin (1000 U/ml), 1% streptomycin (1000 μg/ml) and 1% amphoterycin (250 U/ml). The cells were passaged enzymatically with 0.25% trypsin-1 mM EDTA and sub-cultured on 25 or 75 cm^2 plastic flasks at a density of $2x10^4$ cells cm^{-2}. The culture medium was replaced every 2 days. Cell confluence (80%) was confirmed by microscopic observance. Experiments were performed 24 days post-seeding. Stock solutions of the complexes (saline solution or DMSO) were diluted in complete medium to the required concentration. DMSO at similar concentrations did not show any effects on cytotoxicity.

For cytotoxicity screening experiments, cells were seeded in 96-well plates at a density of $4x10^3$ cells/well. The culture medium was replaced with fresh medium (without FBS) containing the complexes at concentrations varying from 0 to 20 μM, with an exposure time of 72 h. Thereafter, the cell survivals were measured using the MTT test as previously described[56]. The assay is dependent on the cellular reduction of 3-(4,5-dimethyl-2-thiazoyl)-2,5-diphenyltetrazolium bromide (MTT, Merck) by the mitochondrial dehydrogenase of viable cells to a blue formazan product which can be measured spectrophotometrically. Following appropriate incubation of cells, with or without the metallic complexes, MTT was added to each well in an amount equal to 10% of the culture volume and gentle stirring in a gyratory shaker which enhances dissolution and incubation was continued at 37ºC for 4 h. Thereafter the medium and MTT are removed and DMSO is added to each well. At the end, the results are obtained by measuring absorbance with a scanning multiwell spectrophotometer (BIOTEX SINERGY HT SIAFRTD) at wavelength of 560/670 nm and compared to the values of control cells incubated in the absence of complexes. Experiments were conducted in quadruplicate wells and repeated at least three times.

Interaction with bovine serum albumin. BSA was commercially available from Sigma Aldrich. A 1 mM stock solution of BSA was prepared in PBS at pH 7.4. The real concentration is confirmed using UV-Vis spectroscopy ($\varepsilon_{280\,nm}$ = 43824 $M^{-1}cm^{-1}$). Gold complexes were dissolved in DMSO to achieve 6 mM stock solutions and six aliquots of 2.5 μL were added to a 50 μM solution of BSA in PBS placed in a quartz cuvette of 1 cm optical path. The final concentrations of gold complexes in the cuvette were 5, 10, 15, 20, 25 and 30 μM. The fluorescence spectra were recorded on a Jobin-Yvon-Horiba fluorolog FL-3-11 spectrometer. The samples were excited at 295 nm and the emission spectra were recorded in a range from 310 to 450 nm with emission slits set to 2 nm. The samples were measure 240 s after every addition of the aliquots of gold complexes. The fluorescence intensities of the PBS and the gold complexes were irrelevant under the described conditions, as were the effect of addition of gold aliquots and the effect of time incubation between measurements.

The data were analysed using the Stern-Volmer equation $F_0/F = 1 + K_{sv}$[gold complex] = $1 + K_q\tau_0$[gold complex] in order to obtain the Stern-Volmer quenching constant (K_{sv}) and the quenching rate constant (K_q). The binding constant (K_b) was quantified by using the Stern-Volmer equation: $\log\{(F_0-F)/F\} = \log K_b + n\log$[gold complex].

Cell uptake studies and ICP-MS analysis. Cells were seeded in 6-well plates and grown to approximately 70% confluency and incubated with the corresponding metallodrug at 1 μM for 3 h. At the end of the incubation period, cells were rinsed with 5 mL of PBS, detached by adding 0.75 mL trypsin solution and collected by centrifugation and suspended in 2mL of PBS. Cells were lysed by a freezing-thawing technique that was recently found to be suitable for cell uptake studies.[89] All samples were analyzed for their cells content prior to ICP-MS determination. All samples were digested in *aqua regia* for 3 h at room temperature and filled to a total volume of 25 ml with ultrapure water. Determinations of total gold contents were measured using a mass spectrometer (Perkin Elmer Elan DRC-e) equipped with a plasma ICP ion source (ICP-MS).

Measurements of apoptosis. Human HCT-116-luc2 cells were exposed to 20 μM of the metallic compounds for 72 h, then collected and stained with Annexin V-FTIC according to the manufacturer's instructions. A negative control was prepared containing unreacted cells in order to define the basal level of apoptotic and necrotic or dead cells. After incubation, cells were transferred to flow-cytometry tubes and washed twice with temperate phosphate-buffered saline (PBS), resuspended in 100 μL annexin V binding buffer (10 mM Hepes/NaOH, pH 7.4, 140 mM NaCl, 2.5 mM $CaCl_2$), then 5 μL of annexin V-FITC and 5μL of PI was to each 100 μL of cell suspension. After incubation for 15 minutes at room temperature in the dark, 400 μL of 1X annexin binding buffer was added and analyzed by flow cytometry within one hour. The signal intensity was

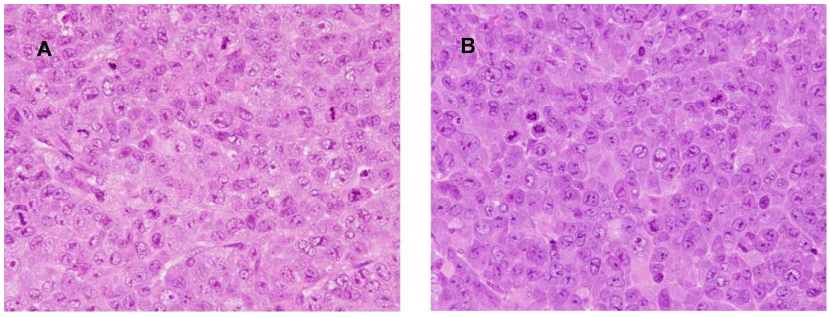

Figure 10. Section of tumour from control mouse (A) and treated mouse with complex **5** (B). Both tumours show similar characteristics with neoplastic epithelial cells of solid growth and a lot of mitosis. H. & E. X 400.

View Article Online
DOI: 10.1039/C5DT01802A

measured using a FACSARIA BD and analyzed using FASCDIVA BD.

Cell cycle analysis. Human HCT-116-luc2 cells were exposed to 20 μM of the metallic compounds for 72 h. The cells were then fixed in 70% ice-cold ethanol and stored at 4 ºC for 24 h. After centrifugation, the cells were rehydrated in PBS (phosphate buffered saline) and stained with propidium iodide (PI, 50 μg/mL) solution containing RNase A (100μg/mL). PI-stained cells were analyzed for DNA content in a FACSARRAY BD equipped with an argon ion laser. The red fluorescence emitted by PI was collected using a 620 nm longer pass filter as a measure of the amount of DNA-bound PI and displayed on a linear scale. Cell cycle distribution was determined on a linear scale. The percentage of cells in cycle phases was determined using MODIFIT 3.0 verity software.

In vivo gold excretion studies. Twenty one CD1 mice (Harlan) weighting between 10 and 20 g were administrated a single intraperitoneal injection of [Au(C≡CCH$_2$Spyridine)(PTA)] (**5**) 5mg/kg -bw- and placed in a metabolic cage. Urine and blood samples were collected over 48 h (at 15, 30, 90 min; 3, 6, 24 and 48 h). The animals were then sacrificed under anaesthesia and CO_2 atmosphere and the corresponding gold contents measured using a mass spectrometer (Perkin Elmer Elan DRC-e) equipped with a plasma ICP ion source (ICP-MS).

In vivo athymic nude mice experiment with HCT-116-luc 2 cells (efficacy study). Eight week old athymic nude mice with no signs of infection (Hsd: Athymic Nude-Foxn1nu/un), weighing approximately 20-22 g, were purchased from Harlan Laboratories, Barcelona (Spain). Mice were individually housed in sterile filter top cages *(1264C Eurostandard Type II.* Techniplast*)* under controlled temperature and lighting (12 h light / 12 h dark) with free access to water and food, and they were fed a normal chow diet (TD2018; Harlan Teklad). Study protocols were approved by the Ethics Committee for Animal Research of the University of Zaragoza (PI02/10).

For evaluation of the antitumour efficacy, mice were injected subcutaneously with HCT-116-luc2 cells (500000 in 300μL) and housed under sterile conditions. The resulting subcutaneous tumours were monitored by optical imaging. [Au(C≡CCH$_2$Spyridine)(PTA)] (**5**) at concentration of 5mg/kg -bw- was administrated intraperitoneally three times weekly (on alternative days). Untreated animals were used as a control (treated only with vehicle solution, DMSO). Each group consisted of six mice. The body weight of each animal was also recorded and their behaviour monitored daily. Animals were treated once the tumour size had reached a mean volume of about 200 mm^3 (tumour volume was calculated as length x width x height and measured daily using a calliper). All animals were euthanized by CO_2 inhalation followed by cervical dislocation at a tumour volume of 1 cm^3 and a necropsy, including livers and kidneys, performed to detect any possibly significant toxic effects, including the presence of any necrotic tissue.

Median survival time (MST) and percentage increase life span (ILS). The effect of [Au(C≡CCH$_2$Spyridine)(PTA)] on tumour growth was also determined as MST and % ILS. The MST for each group of six nude mice was calculated by recording the mortality ("end point") daily for 40 days, with the "end point" of the experiment being taken to be a tumour volume of 1000 mm^3. The % ILS was calculated according to the following equation[90]: %ILS = [{MST$_{treated\ group}$/MST$_{control\ group}$}-1]x100, where MST = (Day of first death + Day of last death)/2

Bioluminescence imaging of tumour growth in vivo. HCT-116 cells were transfected with a luciferase-overexpressing plasmid. Luciferase-overexpressing cells (HCT-116-luc2) were subsequently injected into the nude mice subcutaneously as described above. During the study the mice underwent optical imaging using an IVIS® Lumina Calliper every three days. Ten minutes prior to imaging, each mouse was injected intraperitoneally with 300 μL D-luciferin solution (15 μg/ml in PBS working solution). During imaging, mice were anesthetized with isoflurane (2%).

Statistical Analysis. All results are expressed as means ± SE. Means were compared using one-way analysis of variance (ANOVA). Significant differences at $p<0.05$ were compared using a Bonferroni's Multiple Comparison Test. The statistical analysis and the graphics were performed using the GraphPad Prism Version 5.02 program on a PC computer.

Histology. Kidneys, liver and tumours from all groups of mice were weighed and the relative organ weights were calculated. They were collected, fixed in 10% formaldehyde solution and preserved. Representative sections of the collected tissues were prepared, routinely embedded in paraffin, cut into thick sections and stained with hematoxilin and eosin for the subsequent histopathological examination.

Conclusions

A series of organometallic gold (I) derivatives with the water soluble phosphanes PTA and DAPTA have been described and tested against the human colon cancer cell line Caco-2 (PD7 and TC7 clones). A difference in the antiproliferative activity was found depending on the phosphane, with more effectiveness for the PTA compounds. None significant influence of the substituent in the thiolate unit of the alkyne ligand was found in these PTA complexes. However, the presence of two methyl groups in the DAPTA partners shows moderate increase of cytotoxicity in the PD7 clones. All the complexes display some relevant time-dependent changes in solution under physiological medium that implies that they are acting as pro-drugs. Preliminary cell uptake experiments shows values around 2369 and 3272 pmol/10^6 cells for PTA derivatives (**5** and **7** respectively) and lower values for the DAPTA derivative (**8**) that is in accordance with higher cytotoxic activity of the formers. Moderate values of binding constant were calculated for the interaction of the complexes with bovine serum albumin (BSA), which may imply their transport by this protein in the body and an easy released to the target. The thermodynamic parameters determined for complex [Au(C≡CCH$_2$Spyridine)(PTA)] suggested to the presence of van der Waals interactions or hydrogen bonding between the metallic complex and the protein. Further studies on

View Article Online
DOI: 10.1039/C5DT01802A

complex [Au(C≡CCH$_2$Spyridine)(PTA)] have confirmed its anticancer activity against colon cancer cell lines by apoptotic pathway, by induction S-phase arrest in cell cycle, an increase in mean survival time (MST) and life expectancy in athymic nude mice xenografted with human HCT-116-luc2 cancer cells and moderate inhibition tumour growth without acute toxicity.

Acknowledgements

Authors thank to Centro de Investigación Biomédica de Aragón (CIBA), España for technical assistance: http://www.iacs.aragon.es, *use of Servicio General de Apoyo a la Investigación-SAI, Universidad de Zaragoza and* to Torrecid S.A. for a generous donation of H[AuCl$_4$]. We also thank to José A. García de Jalón for the pictures obtained in the histopathological examination.

Notes and references

1. K. R. Barnes and S. J. Lippard, *Metal Ions in Biolgical Systems, Vol 42: Metal Complexes in Tumor Diagnosis and as Anticancer Agents*, 2004, **42**, 143-177.
2. Y. Kim, S. Park, J. Park, E. Cho, D. Shin and J. Lee, *J. Clin. Oncol.*, 2008, **26**, supp. 4577.
3. A. A. Argyriou, P. Polychronopoulos, G. Iconomou, E. Chroni and H. P. Kalofonos, *Cancer Treatment Rev.*, 2008, **34**, 368-377.
4. N. Muhammad and Z. Guo, *Current Opinion Chem. Biol.*, 2014, **19**, 144-153.
5. M. R. Gill and J. A. Thomas, *Chem. Soc. Rev.*, 2012, **41**, 3179-3192.
6. A. Bergamo, C. Gaiddon, J. H. M. Schellens, J. H. Beijnen and G. Sava, *J. Inorg. Biochem.*, 2012, **106**, 90-99.
7. C. G. Hartinger, A. D. Phillips and A. A. Nazarov, *Current Topics in Medicinal Chemistry*, 2011, **11**, 2688-2702.
8. S. K. Singh and D. S. Pandey, *RSC Advances*, 2014, **4**, 1819-1840.
9. S. Komeda and A. Casini, *Current Topics in Medicinal Chemistry*, 2012, **12**, 219-235.
10. G. N. Kaluderovic and R. Paschke, *Current Med. Chem.*, 2011, **18**, 4738-4752.
11. K. B. Garbutcheon-Singh, M. P. Grant, B. W. Harper, A. M. Krause-Heuer, M. Manohar, N. Orkey and J. R. Aldrich-Wright, *Current Topics in Medicinal Chemistry*, 2011, **11**, 521-542.
12. I. Kostova, *Anti-Cancer Agents Med. Chem.*, 2009, **9**, 827-842.
13. C. Nardon, G. Boscutti and D. Fregona, *Anticancer Res.*, 2014, **34**, 487-492.
14. N. Cutillas, G. S. Yellol, C. de Haro, C. Vicente, V. Rodriguez and J. Ruiz, *Coord. Chem. Rev.*, 2013, **257**, 2784-2797.
15. L. Oehninger, R. Rubbiani and I. Ott, *Dalton Trans.*, 2013, **42**, 3269-3284.
16. J. S. Butler and P. J. Sadler, *Curr. Opin. Chem. Biol.*, 2013, **17**, 175-188.
17. C. Gabbiani, M. A. Cinellu, L. Maiore, L. Massai, F. Scaletti and L. Messori, *Inorg. Chim. Acta*, 2012, **393**, 115-124.
18. S. J. Berners-Price and A. Filipovska, *Metallomics*, 2011, **3**, 863-873.
19. C. M. Che and R. W. Y. Sun, *Chem. Commun.*, 2011, **47**, 9554-9560.
20. A. Casini, C. Hartinger, C. Gabbiani, E. Mini, P. J. Dyson, B. K. Keppler and L. Messori, *J. Inorg. Biochem.*, 2008, **102**, 564-575.
21. S. Nobili, E. Mini, I. Landini, C. Gabbiani, A. Casini and L. Messori, *Med. Res. Rev.*, 2010, **30**, 550-580.
22. C. Gabbiani, A. Casini and L. Messori, *Gold Bull. (London, U. K.)*, 2007, **40**, 73-88.
23. A. Casini and L. Messori, *Curr. Top. Med. Chem.* , 2011, **11**, 2647-2660.
24. E. M. Nagy, L. Ronconi, C. Nardon and D. Fregona, *Mini-Rev. Med. Chem.*, 2012, **12**, 1216-1229.
25. A. Mukherjee and P. J. Sadler, eds., *Metals in medicine: therapeutic agents.*, John Wiley & Sons, Inc., 2009.
26. C. Nardon, S. M. Schmitt, H. J. Yang, J. Zuo, D. Fregona and Q. P. Dou, *PLoS One*, 2014, **9**.
27. A. Korfel, M. E. Scheulen, H. J. Schmoll, O. Grundel, A. Harstrick, M. Knoche, L. M. Fels, M. Skorzec, F. Bach, J. Baumgart, G. Sass, S. Seeber, E. Thiel and W. E. Berdel, *Clin. Cancer Res.*, 1998, **4**, 2701-2708.
28. G. Lummen, H. Sperling, H. Luboldt, T. Otto and H. Rubben, *Cancer Chemother. Pharmacol.*, 1998, **42**, 415-417.
29. E. Melendez, *Crit. Rev. Oncol. Hematol.*, 2002, **42**, 309-315.
30. A. Bergamo, B. Gava, E. Alessio, G. Mestroni, B. Serli, M. Cocchietto, S. Zorzet and G. Sava, *Int. J. Oncol.*, 2002, **21**, 1331-1338.
31. C. G. Hartinger, S. Zorbas-Seifried, M. A. Jakupec, B. Kynast, H. Zorbas and B. K. Keppler, *J. Inorg. Biochem.*, 2006, **100**, 891-904.
32. A. Bergamo, A. Masi, P. J. Dyson and G. Sava, *Int. J. Oncol.*, 2008, **33**, 1281-1289.
33. P. Nowak-Sliwinska, J. R. van Beijnum, A. Casini, A. A. Nazarov, G. Wagnieres, H. van den Bergh, P. J. Dyson and A. W. Griffioen, *J. Med. Chem.*, 2011, **54**, 3895-3902.
34. C. S. Allardyce, A. Dorcier, C. Scolaro and P. J. Dyson, *Appl. Organomet. Chem.*, 2005, **19**, 1-10.
35. C. G. Hartinger and P. J. Dyson, *Chem. Soc. Rev.*, 2009, **38**, 391-401.
36. G. Gasser, I. Ott and N. Metzler-Nolte, *J. Med. Chem.*, 2011, **54**, 3-25.
37. G. Gasser and N. Metzler-Nolte, *Current Opinion Chem. Biol.*, 2012, **16**, 84-91.
38. B. Bertrand and A. Casini, *Dalton Trans.*, 2014, **43**, 4209-4219.
39. C. G. Hartinger, N. Metzler-Nolte and P. J. Dyson, *Organometallics*, 2012, **31**, 5677-5685.
40. E. Melendez, *Inorg. Chim. Acta*, 2012, **393**, 36-52.
41. S. S. Braga and A. M. S. Silva, *Organometallics*, 2013, **32**, 5626-5639.
42. S. Gomez-Ruiz, D. Maksimovic-Ivanic, S. Mijatovic and G. N. Kaluderovic, *Bioinorg. Chem. Appl.*, 2012, DOI: 10.1155/2012/140284.
43. M. Hanif, M. V. Babak and C. G. Hartinger, *Drug Discovery Today*, 2014, **19**, 1640-1648.
44. M. Patra, G. Gasser, A. Pinto, K. Merz, I. Ott, J. E. Bandow and N. Metzler-Nolte, *ChemMedChem*, 2009, **4**, 1930-1938.
45. I. Ott, *Coord. Chem. Rev.*, 2009, **253**, 1670-1681.

View Article Online
DOI: 10.1039/C5DT01802A

46. B. Bertrand, E. Bodio, P. Richard, M. Picquet, P. Le Gendre and A. Casini, *J. Organomet. Chem.*, 2015, **775**, 124-129.
47. B. Bertrand, A. de Almeida, E. P. M. van der Burgt, M. Picquet, A. Citta, A. Folda, M. P. Rigobello, P. Le Gendre, E. Bodio and A. Casini, *Eur. J. Inorg. Chem.*, 2014, DOI: 10.1002/ejic.201402248, 4532-4536.
48. J. Arcau, V. Andermark, M. Rodrigues, I. Giannicchi, L. Perez-Garcia, I. Ott and L. Rodriguez, *Eur. J. Inorg. Chem.*, 2014, 6117-6125.
49. B. Bertrand, S. Spreckelmeyer, E. Bodio, F. Cocco, M. Picquet, P. Richard, P. Le Gendre, C. Orvig, M. A. Cinellu and A. Casini, *Dalton Trans.*, 2015, **44**, 11911-11918.
50. E. Vergara, E. Cerrada, A. Casini, O. Zava, M. Laguna and P. J. Dyson, *Organometallics*, 2010, **29**, 2596-2603.
51. E. Schuh, S. M. Valiahdi, M. A. Jakupec, B. K. Keppler, P. Chiba and F. Mohr, *Dalton Trans.*, 2009, 10841-10845.
52. A. Meyer, C. P. Bagowski, M. Kokoschka, M. Stefanopoulou, H. Alborzinia, S. Can, D. H. Vlecken, W. S. Sheldrick, S. Wolfl and I. Ott, *Angew. Chem. Int. Ed. Engl.*, 2012, **51**, 8895-8899.
53. D. Zhang, Z. Xu, J. Yuan, Y.-X. Zhao, Z.-Y. Qiao, Y.-J. Gao, G.-A. Yu, J. Li and H. Wang, *J. Med. Chem.*, 2014, **57**, 8132-8139.
54. J. Arcau, V. Andermark, E. Aguilo, A. Gandioso, A. Moro, M. Cetina, J. C. Lima, K. Rissanen, I. Ott and L. Rodriguez, *Dalton Transactions*, 2014, **43**, 4426-4436.
55. V. Andermark and I. Ott, *J. Biol. Inorg. Chem.*, 2014, **19**, S791-S792.
56. E. Garcia-Moreno, S. Gascon, M. J. Rodriguez-Yoldi, E. Cerrada and M. Laguna, *Organometallics*, 2013, **32**, 3710-3720.
57. E. García-Moreno, S. Gascón, E. Atrián-Blasco, M. J. Rodriguez-Yoldi, E. Cerrada and M. Laguna, *Eur. J. Med. Chem.*, 2014, **74**, 164-172.
58. E. García-Moreno, E. Cerrada, M. J. Bolsa, A. Luquin and M. Laguna, *Eur. J. Inorg. Chem.*, 2013, 2020-2030.
59. E. Vergara, E. Cerrada, C. Clavel, A. Casini and M. Laguna, *Dalton Trans.*, 2011, **40**, 10927-10935.
60. E. Vergara, A. Casini, F. Sorrentino, O. Zava, E. Cerrada, M. P. Rigobello, A. Bindoli, M. Laguna and P. J. Dyson, *ChemMedChem*, 2010, **5**, 96-102.
61. F. Mohr, A. Mendia and M. Laguna, *Eur. J. Inorg. Chem.*, 2007, 3115-3123.
62. I. Chantret, A. Rodolosse, A. Barbat, E. Dussaulx, E. Brotlaroche, A. Zweibaum and M. Rousset, *J Cell Science*, 1994, **107**, 213-225.
63. U. Kragh-Hansen, *Pharmacol. Rev.*, 1981, **33**, 17-53.
64. A. R. Timerbaev, C. G. Hartinger, S. S. Aleksenko and B. K. Keppler, *Chem. Rev.*, 2006, **106**, 2224-2248.
65. X. Y. Yu, Y. Yang, X. Zou, H. W. Tao, Y. L. Ling, Y. Qing, H. Zhou and P. G. Yi, *Spectrochim. Acta A*, 2012, **94**, 23-29.
66. K. Yamasaki, T. Maruyama, U. KraghHansen and M. Otagiri, *Biochim. Biophys. Acta*, 1996, **1295**, 147-157.
67. M. Ganeshpandian, S. Ramakrishnan, M. Palaniandavar, E. Suresh, A. Riyasdeen and M. A. Akbarsha, *J. Inorg. Biochem.*, 2014, **140**, 202-212.
68. C. D. Sanghvi, P. M. Olsen, C. Elix, S. Peng, D. S. Wang, Z. Chen, D. M. Shin, K. I. Hardcastle, C. E. MacBeth and J. F. Eichler, *J. Inorg. Biochem.*, 2013, **128**, 68-76.
69. M. Carreira, R. Calvo-Sanjuan, M. Sanau, X. B. Zhao, R. S. Magliozzo, I. Marzo and M. Contel, *J. Inorg. Biochem.*, 2012, **116**, 204-214.
70. H. L. Yue, Y. J. Hu, J. Chen, A. M. Bai and Y. Ouyang, *Colloids Surf. B*, 2014, **122**, 107-114.
71. J. F. Neault and H. A. Tajmir-Riahi, *Biochim. Biophys. Acta-Protein Struct. Molec. Enzym.*, 1998, **1384**, 153-159.
72. L. R. Gouvea, L. S. Garcia, D. R. Lachter, P. R. Nunes, F. D. Pereira, E. P. Silveira-Lacerda, S. R. W. Louro, P. J. S. Barbeira and L. R. Teixeira, *Eur. J. Med. Chem.*, 2012, **55**, 67-73.
73. A. J. Canumalla, S. Schraa, A. A. Isab, C. F. Shaw, E. Gleichmann, L. Dunemann and M. Turfeld, *J. Biol. Inorg. Chem.*, 1998, **3**, 9-17.
74. J. R. Lakowicz, *in 'Principles of fluorescence Spectroscopy'*, Springer, 2006.
75. Y. J. Hu, Y. Liu, R. M. Zhao and S. S. Qu, *Int. J. Biol. Macromol.*, 2005, **37**, 122-126.
76. P. D. Ross and S. Subramanian, *Biochemistry*, 1981, **20**, 3096.
77. L. Maiore, M. A. Cinellu, E. Michelucci, G. Moneti, S. Nobili, I. Landini, E. Mini, A. Guerri, C. Gabbiani and L. Messori, *J. Inorg. Biochem.*, 2011, **105**, 348.
78. C. M. Sorenson, M. A. Barry and A. Eastman, *J. Natl Cancer Inst.*, 1990, **82**, 749-755.
79. S. William-Faltaos, D. Rouillard, P. Lechat and G. Bastian, *Fundam. Clin. Pharmacol.*, 2007, **21**, 165-172.
80. E. A. Harrington, J. L. Bruce, E. Harlow and N. Dyson, *Proc. Nat. Acad. Sci. USA*, 1998, **95**, 11945-11950.
81. C. A. S. Bergstrom, *Basic Clin. Pharmacol. Toxicol.*, 2005, **96**, 156-161.
82. M. A. Sabatino, T. Colombo, C. Geroni, S. Marchini and M. Broggini, *Clin. Cancer Res.*, 2003, **9**, 5402-5408.
83. L. M. Howells, S. Sale, S. N. Sriramareddy, G. R. B. Irving, D. J. L. Jones, C. J. Ottley, D. G. Pearson, C. D. Mann, M. M. Manson, D. P. Berry, A. Gescher, W. P. Steward and K. Brown, *Int. J. Cancer*, 2011, **129**, 476-486.
84. Y. Sun, R. Yin, S. Gou and Z. Jian, *J. Inorg. Biochem.*, 2012, **112**, 68-76.
85. E. García-Moreno, S. Gascón, J. A. G. d. Jalón, E. Romanos, M. J. Rodriguez-Yoldi, E. Cerrada and M. Laguna, *Anti-Cancer Agents Med. Chem.*, 2015, **15**, 773-782.
86. D. J. Daigle, *Inorg. Synth.*, 1999, **32**, 40-42.
87. E. Vergara, S. Miranda, F. Mohr, E. Cerrada, E. R. T. Tiekink, P. Romero, A. Mendia and M. Laguna, *Eur. J. Inorg. Chem.*, 2007, 2926-2933.
88. B. M. Sutton, E. McGusty, D. T. Waltz and M. J. Di Martino, *J. Med. Chem.*, 1972, **15**, 1095-1098.
89. M. Q. T.Tran, Y. Nygren, C. Lundin, P. Naredi and E. Bjorn, *Anal. Biochem.*, 2010, **1**, 76.
90. V. P. Devmurari and N. P. Jivani, *Int. J. Pharm. Tech. Res.*, 2010, **2**, 1603-1608.

View Article Online
DOI: 10.1039/C5DT01802A

In vitro and *in vivo* evaluation of organometallic gold (I) derivatives as anticancer agents.

Elena García-Moreno[a], *Alejandro Tomás*[a], *Elena Atrián-Blasco*[a], *Sonia Gascón*[b], *Eduardo Romanos*[c], *M*[a] *Jesus Rodriguez-Yoldi*[b], *Elena Cerrada*[a] *and Mariano Laguna*[a,*]

[a]*Departamento de Química Inorgánica, Instituto de Síntesis Química y Catálisis Homogénea-ISQCH, Universidad de Zaragoza-C.S.I.C., 50009 Zaragoza, Spain;* [b]*Departamento de Farmacología y Fisiología. Unidad de Fisiología, Facultad de Veterinaria, Universidad de Zaragoza, 50013, Zaragoza, CIBERobn, Spain;*[c]*Instituto Aragonés de Ciencias de la Salud (IACS). Av San Juan Bosco 13, 50009, Zaragoza*

Supporting information

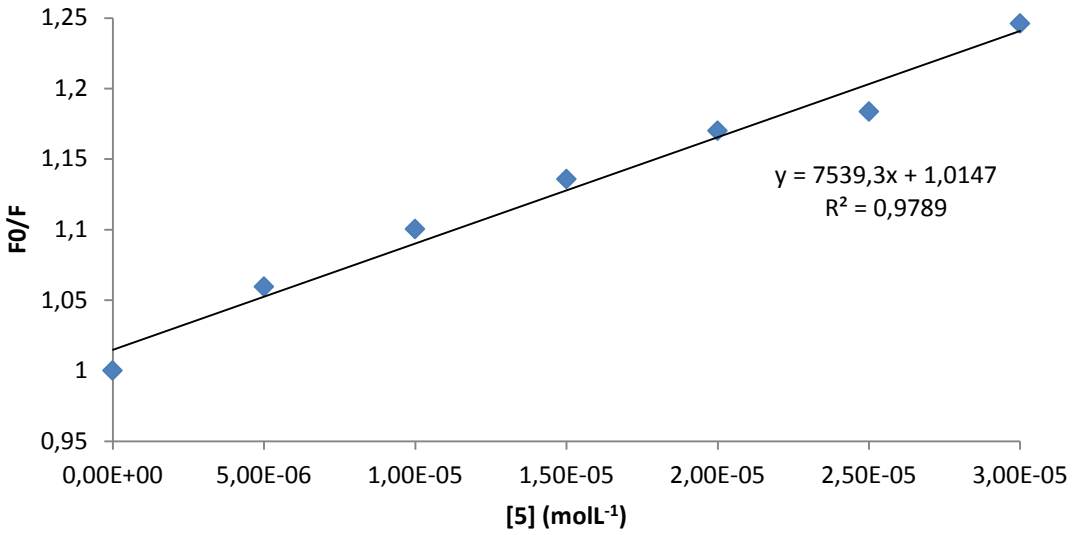

Figure S1. Stern-Volmer plot for the quenching of BSA with complex **5**. Stern-Volmer equation used: $F_0/F = 1 + K_{sv}[5]$.

View Article Online
DOI: 10.1039/C5DT01802A

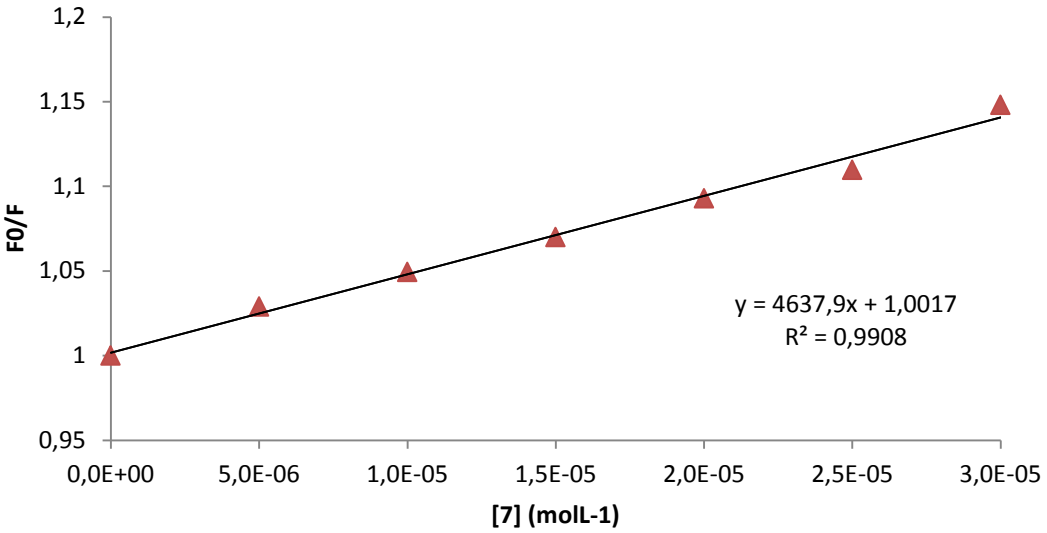

Figure S2. Stern-Volmer plot for the quenching of BSA with complex **7**.

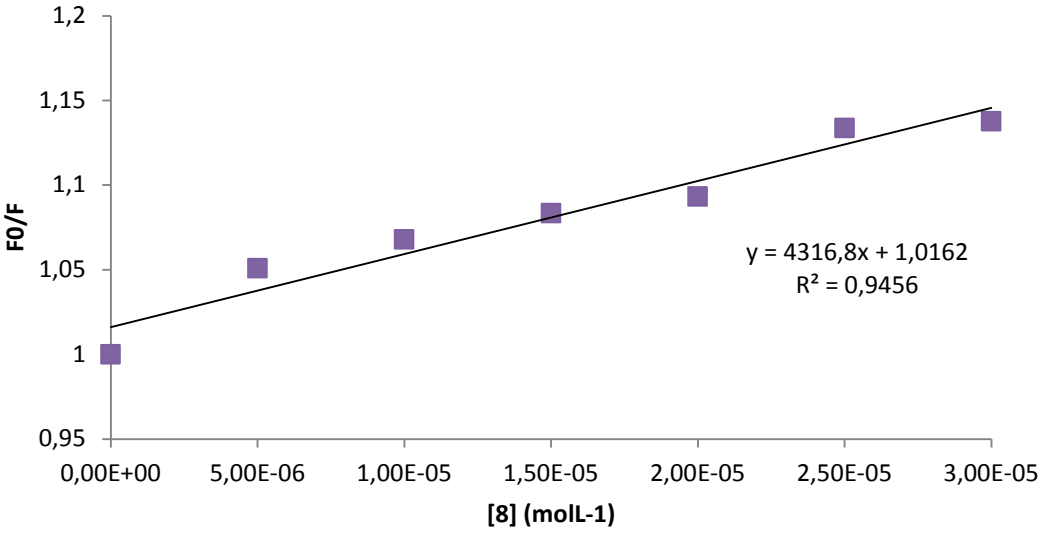

Figure S3. Stern-Volmer plot for the quenching of BSA with complex **8**.

View Article Online
DOI: 10.1039/C5DT01802A

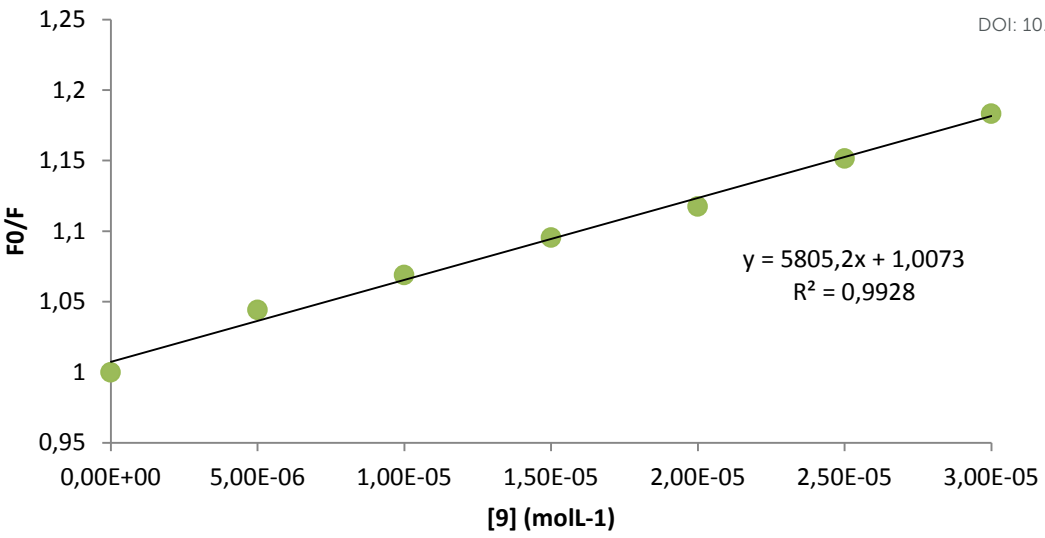

Figure S4. Stern-Volmer plot for the quenching of BSA with complex **9**.

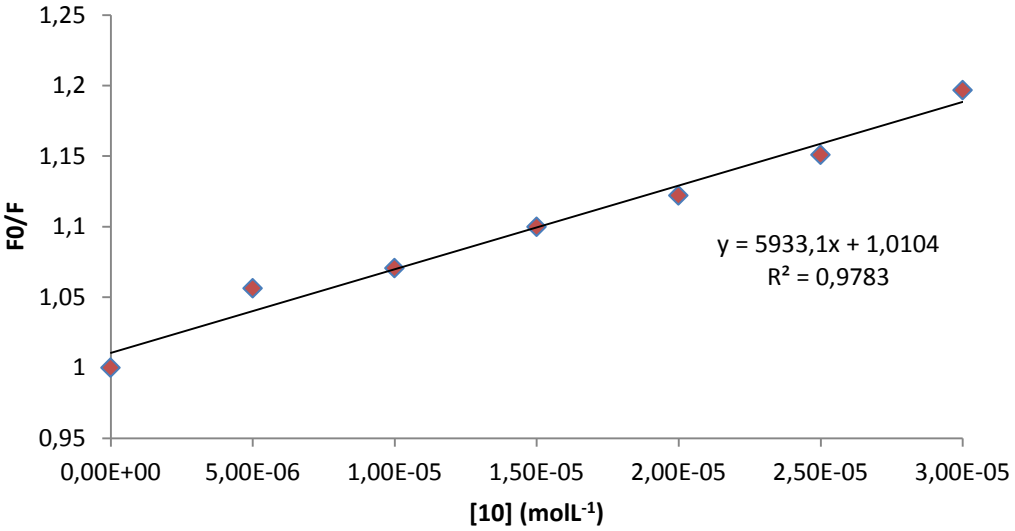

Figure S5. Stern-Volmer plot for the quenching of BSA with complex **10**.

View Article Online
DOI: 10.1039/C5DT01802A

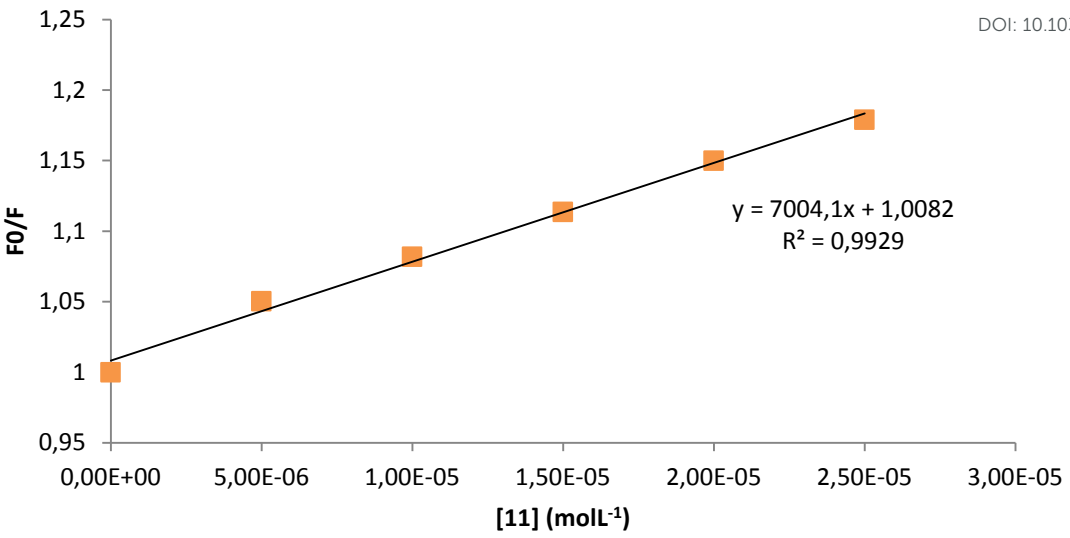

Figure S6. Stern-Volmer plot for the quenching of BSA with complex **11**.

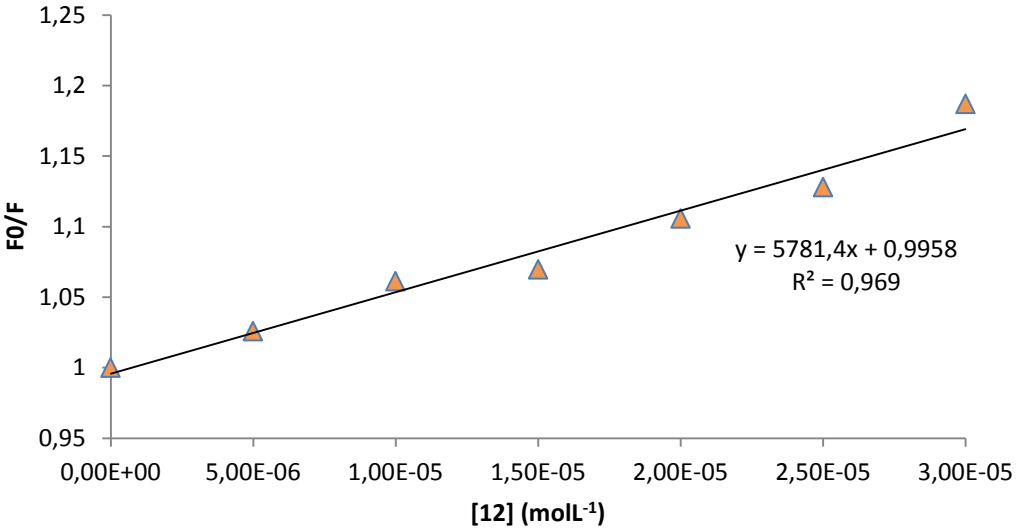

Figure S7. Stern-Volmer plot for the quenching of BSA with complex **12**.

View Article Online
DOI: 10.1039/C5DT01802A

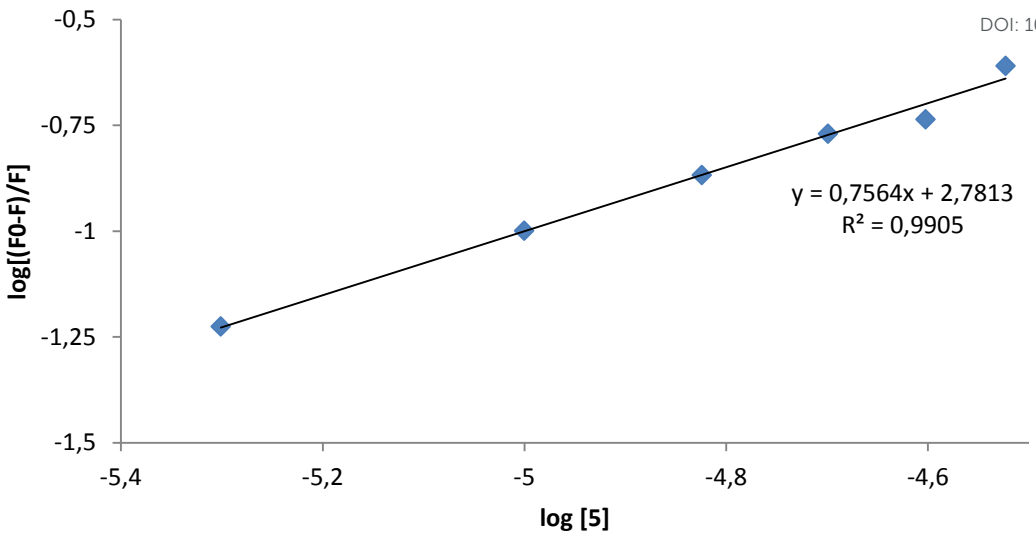

Figure S8. Stern-Volmer equation used: $\log\{(F_0\text{-}F)/F\} = \log K_b + n\log[\mathbf{5}]$. The intercept of the best fit linear trend provides the Stern-Volmer quenching constant K_b.

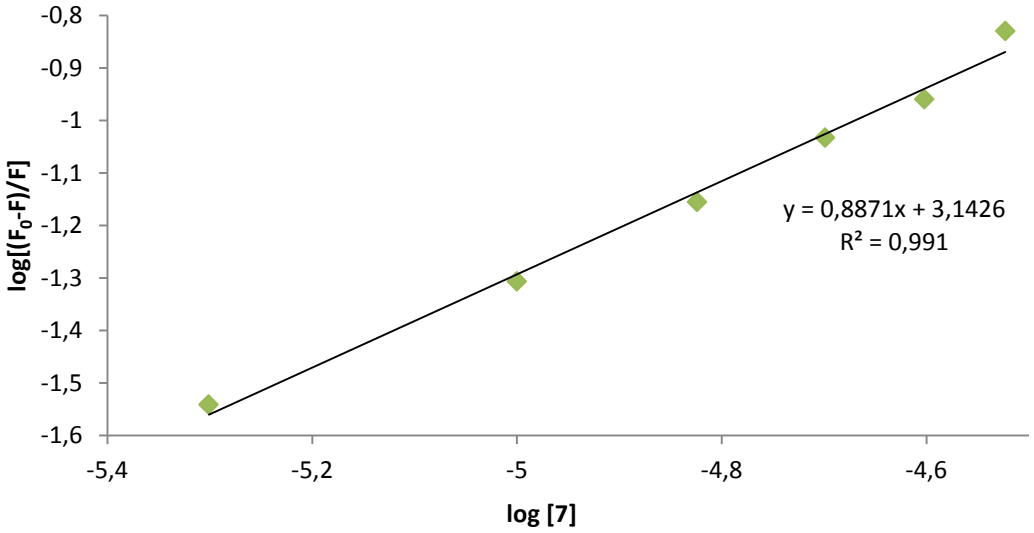

Figure S9. Stern-Volmer plot for the quenching of BSA with complex **7.** Stern-Volmer equation used: $\log\{(F_0\text{-}F)/F\} = \log K_b + n\log[7]$.

View Article Online
DOI: 10.1039/C5DT01802A

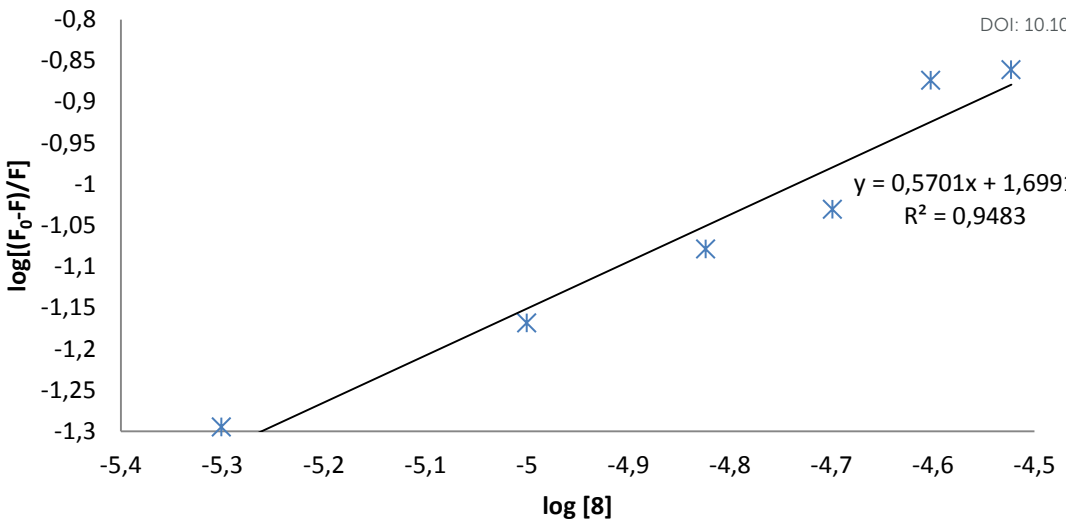

Figure S10. Stern-Volmer plot for the quenching of BSA with complex **8**. Stern-Volmer equation used: $\log\{(F_0\text{-}F)/F\} = \log K_b + n\log[8]$.

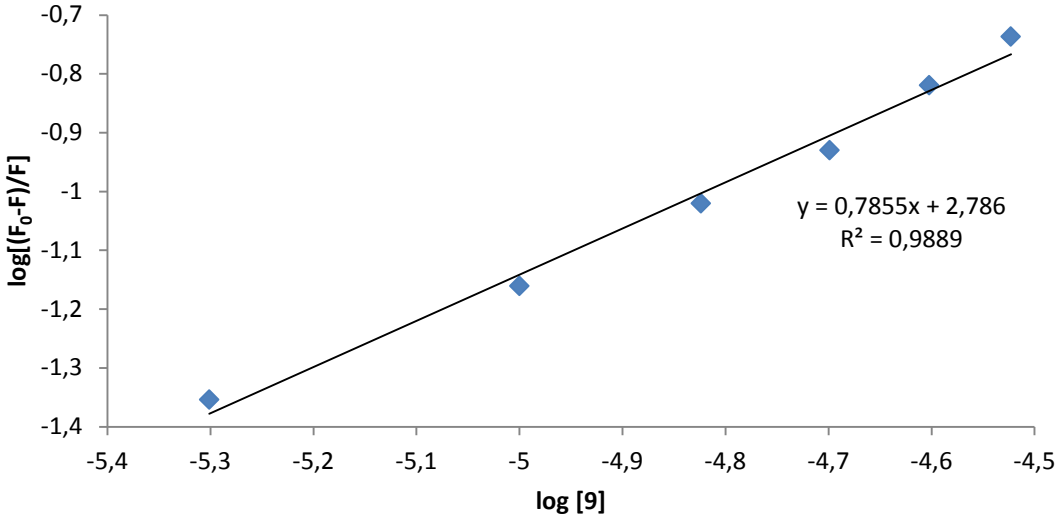

Figure S11. Stern-Volmer plot for the quenching of BSA with complex **9**. Stern-Volmer equation used: $\log\{(F_0\text{-}F)/F\} = \log K_b + n\log[9]$.

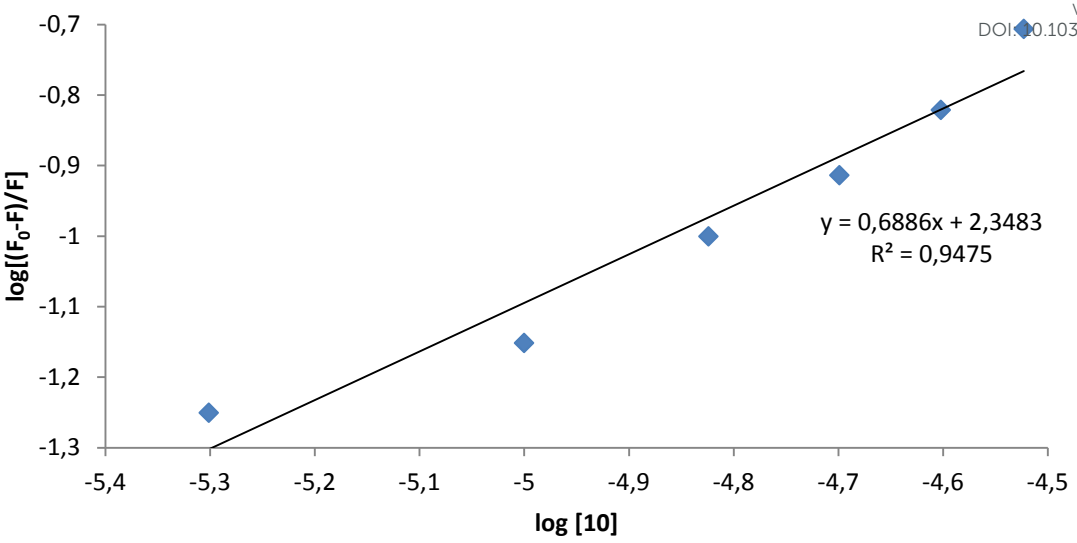

Figure S12. Stern-Volmer plot for the quenching of BSA with complex **10**. Stern-Volmer equation used: $\log\{(F_0\text{-}F)/F\} = \log K_b + n\log [10]$.

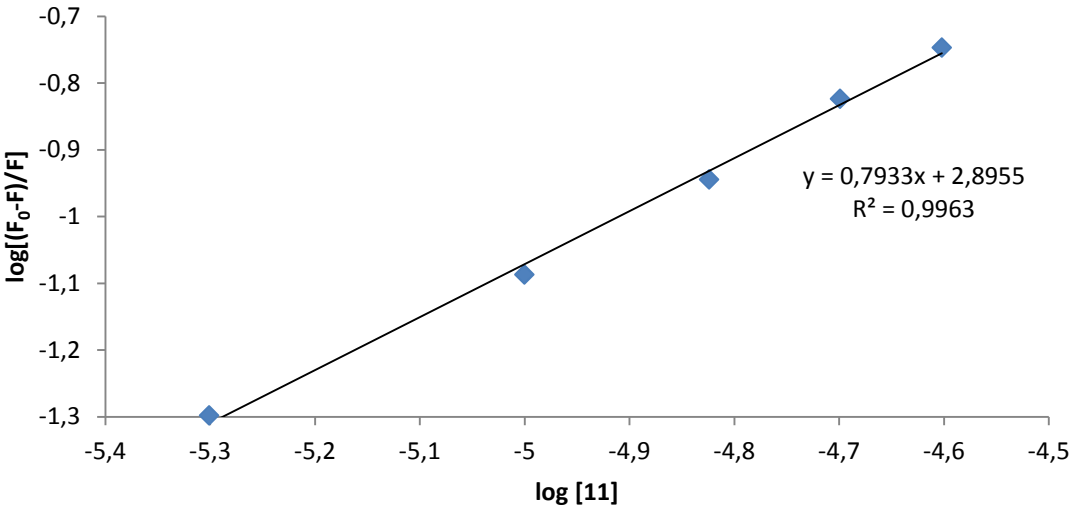

Figure S13. Stern-Volmer plot for the quenching of BSA with complex **11.** Stern-Volmer equation used: $\log\{(F_0\text{-}F)/F\} = \log K_b + n\log [11]$.

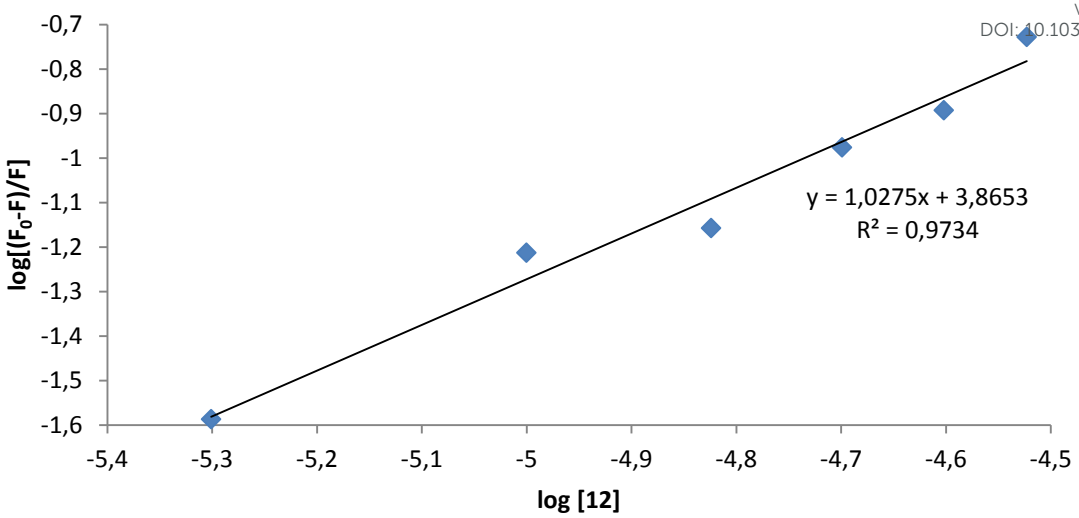

Figure S14. Stern-Volmer plot for the quenching of BSA with complex **12.** Stern-Volmer equation used: $\log\{(F_0\text{-}F)/F\} = \log K_b + n\log [12]$.

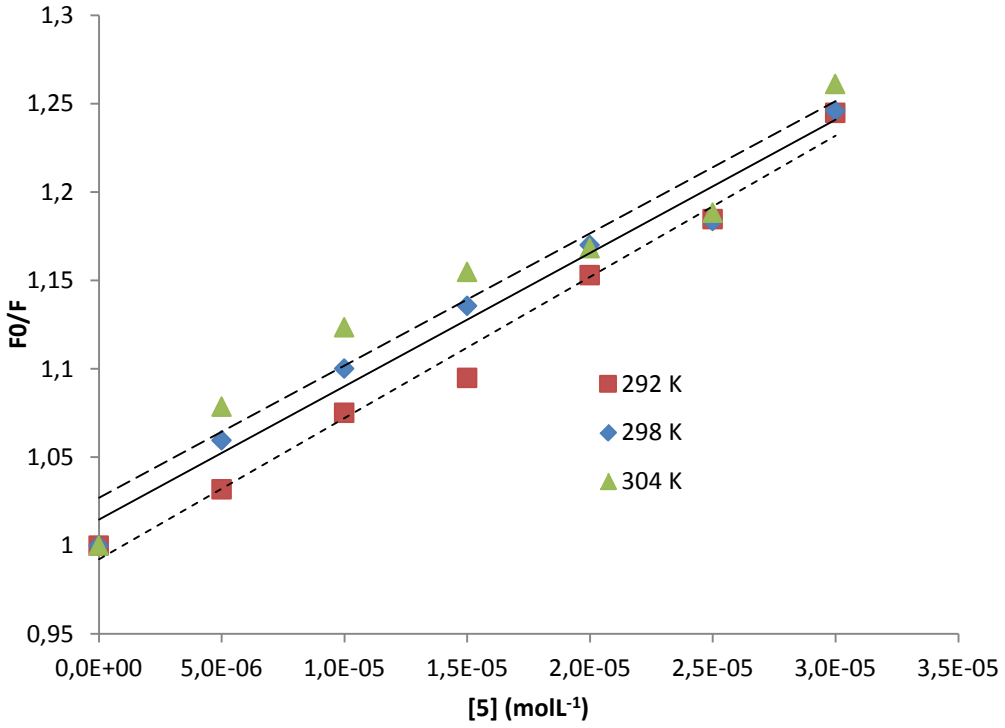

Figure S15. Stern-Volmer plot for the quenching of BSA with complex **5** at different temperatures. Stern-Volmer equation used: $F_0/F = 1 + K_{sv}[5]$.

View Article Online
DOI: 10.1039/C5DT01802A

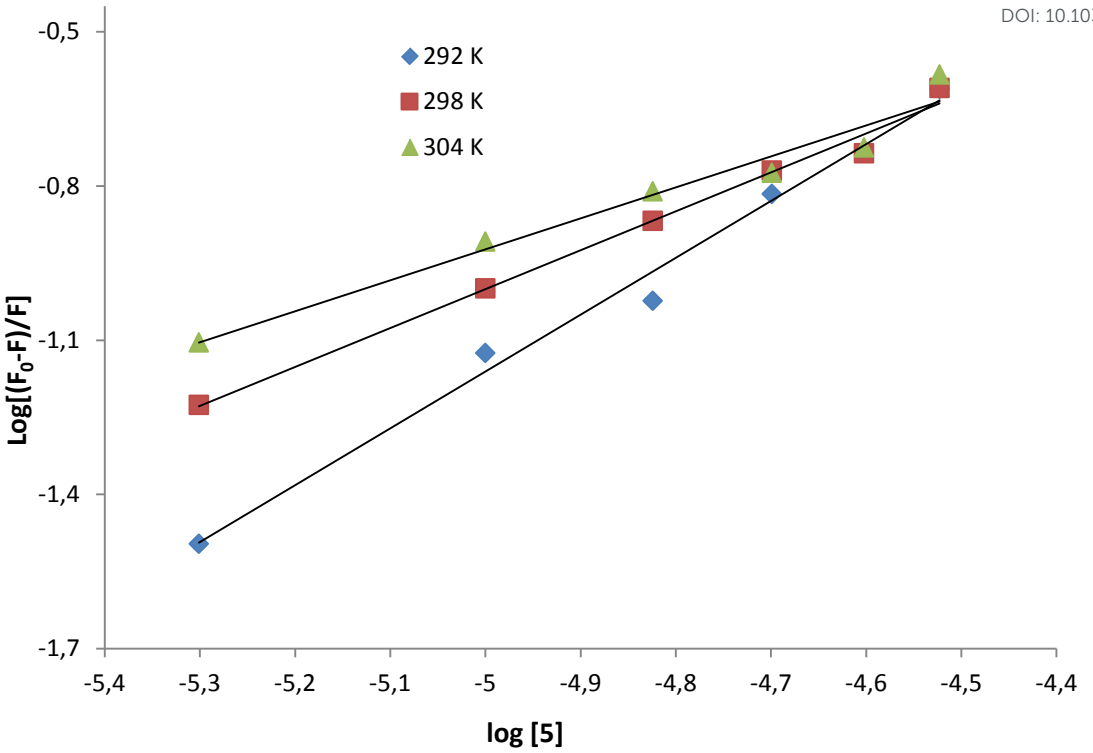

Figure S16. Plot of log{(F_0-F)/F} versus log [**5**] at different temperatures.

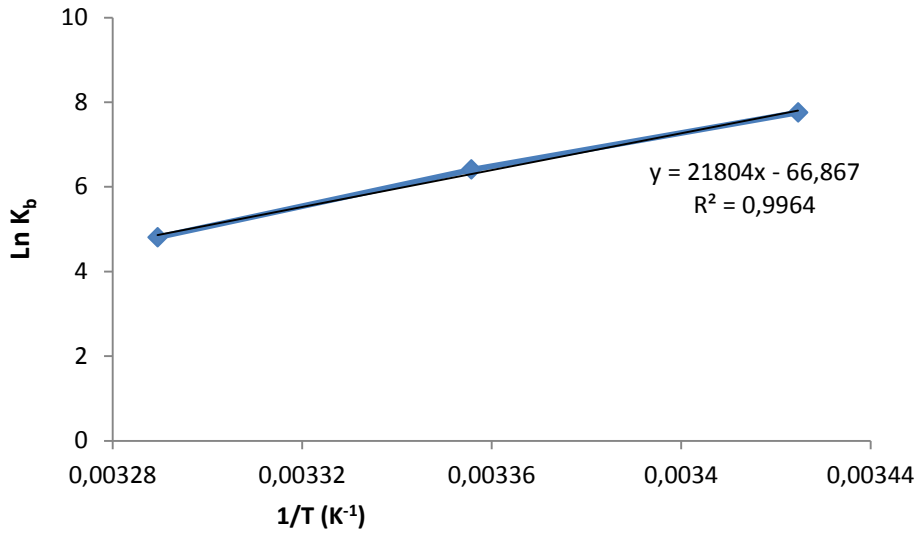

Figure S17. Plot of LnK_b of complex **5** versus 1/T

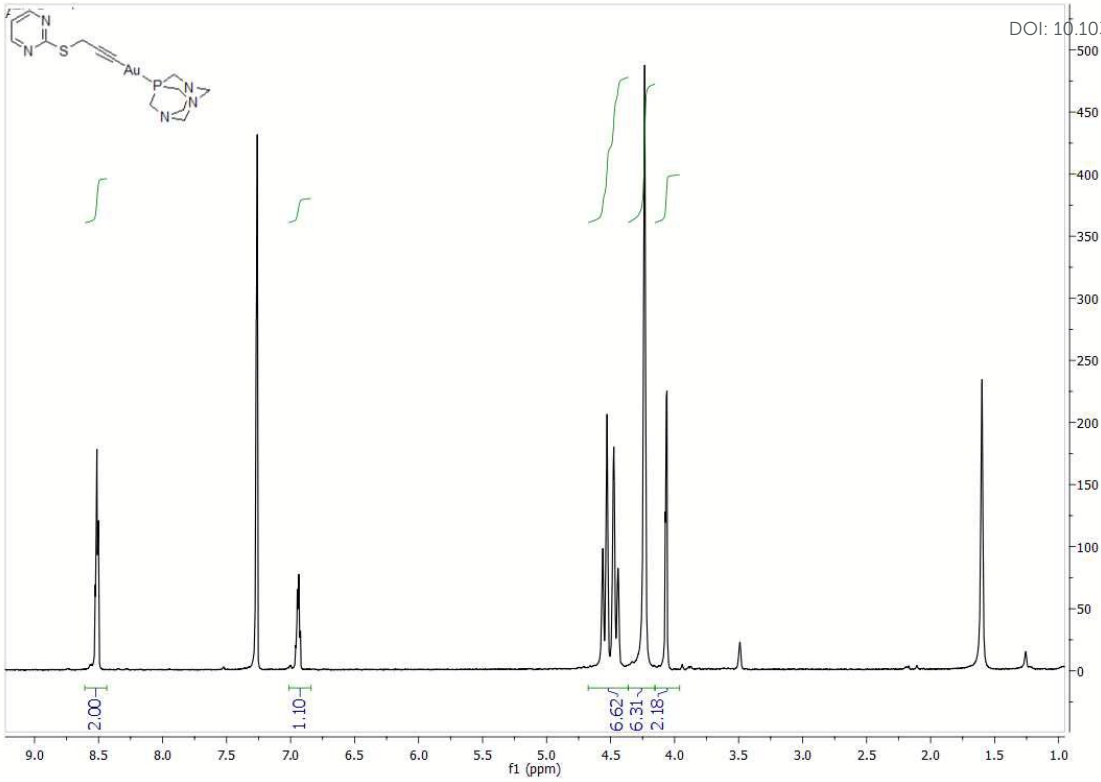

Figure S18. ^{1}H NMR of compound **7**

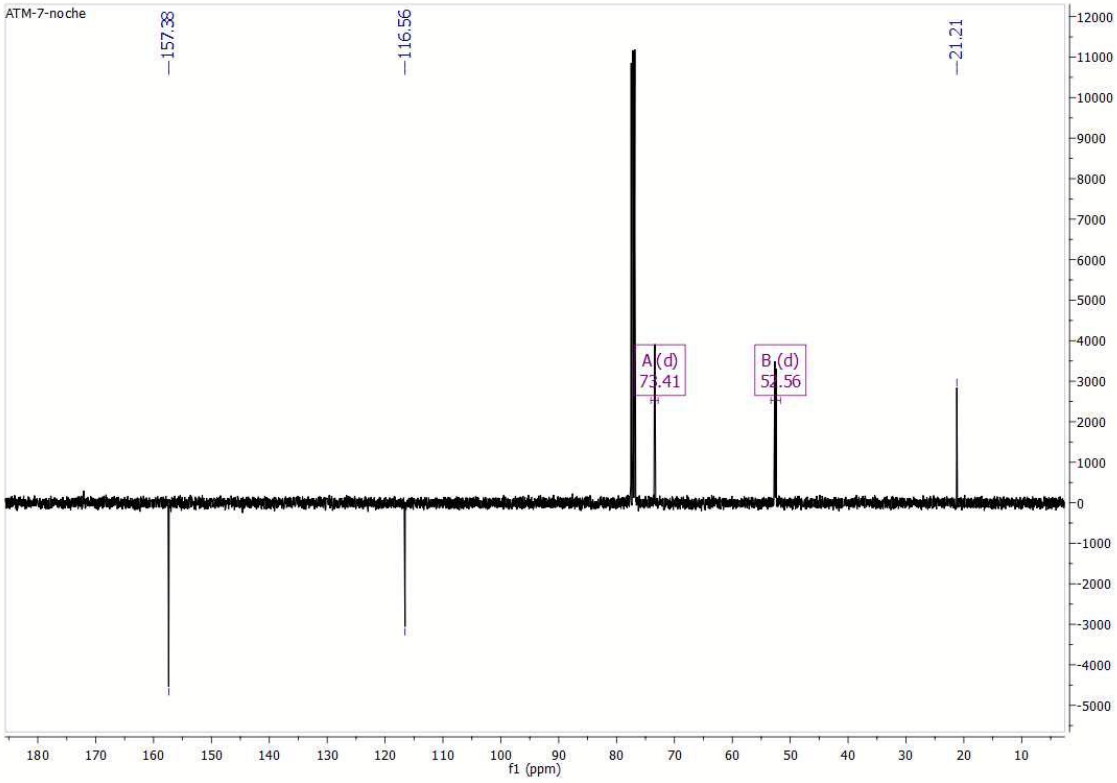

Figure S19. $^{13}C\{^{1}H\}$ NMR of compound **7**

View Article Online
DOI: 10.1039/C5DT01802A

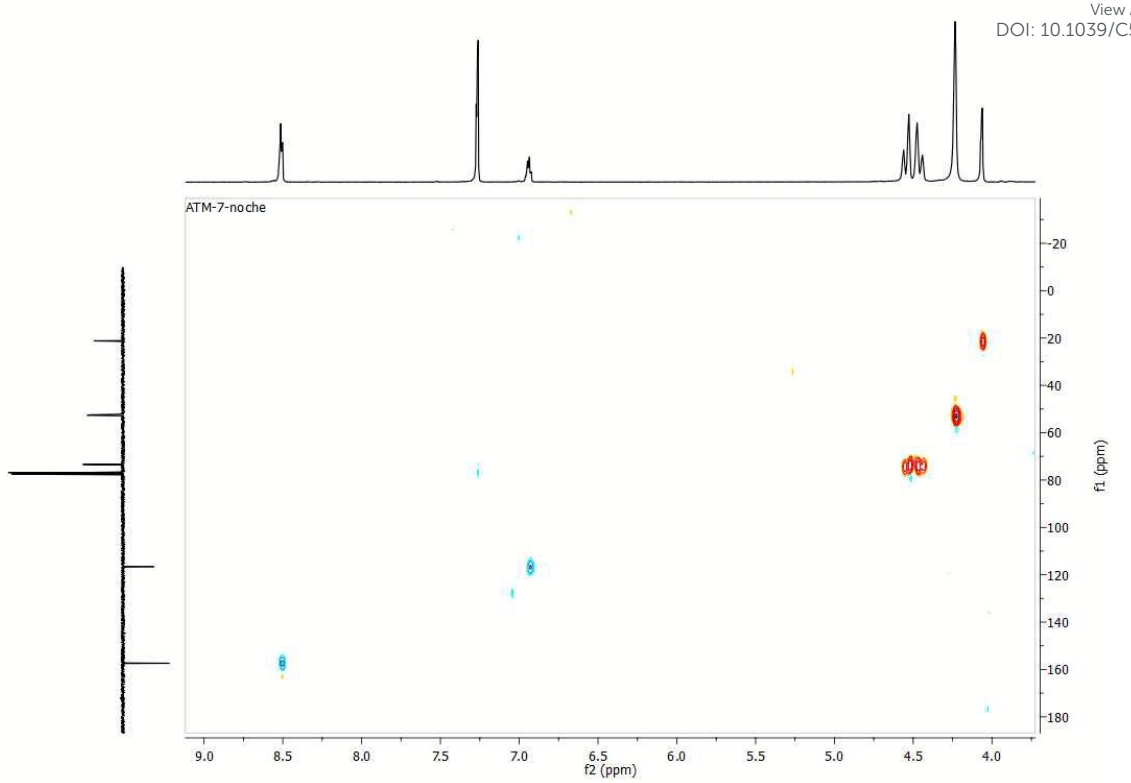

Figure S20. C,H-HSQC NMR of compound **7**

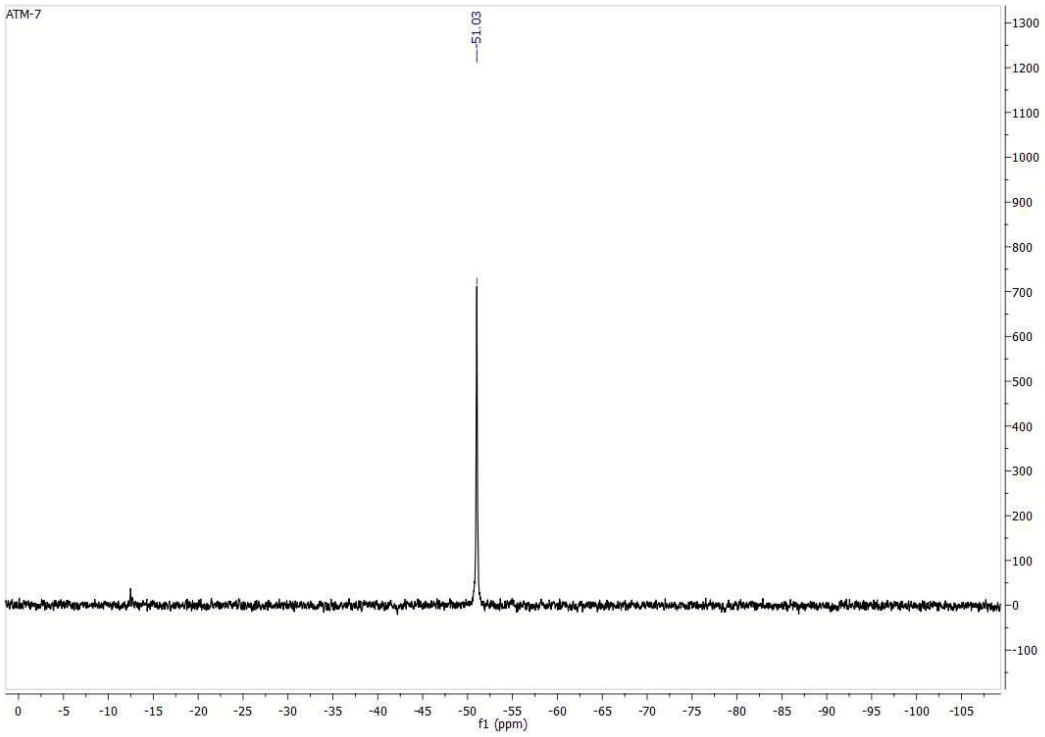

Figure S21. $^{31}P\{^{1}H\}$ NMR of compound **7**

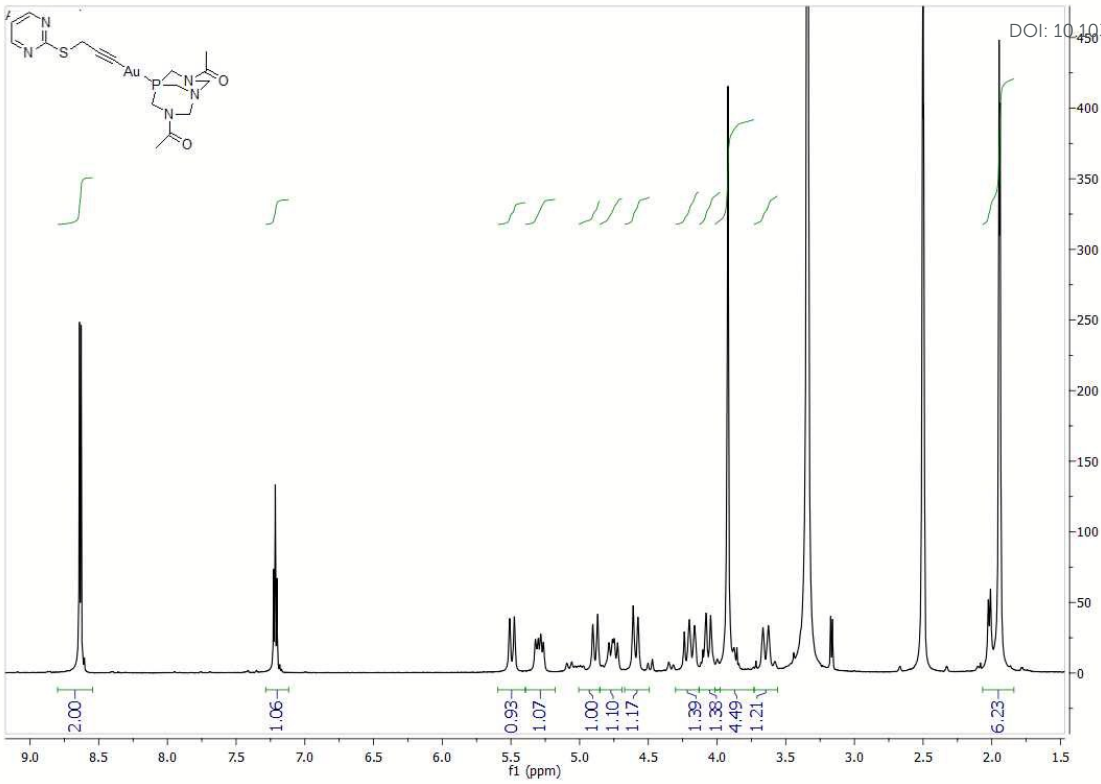

Figure S22. ^{1}H NMR of compound **8**

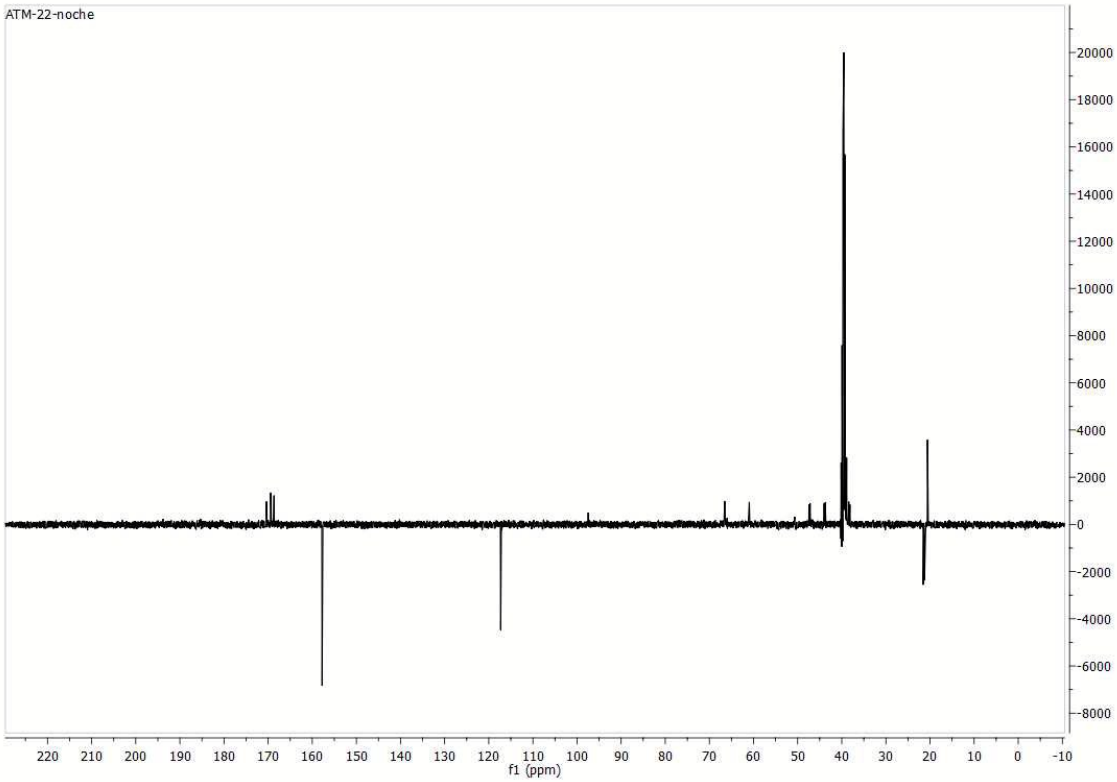

Figure S23. ^{13}C{^{1}H} NMR of compound **8**

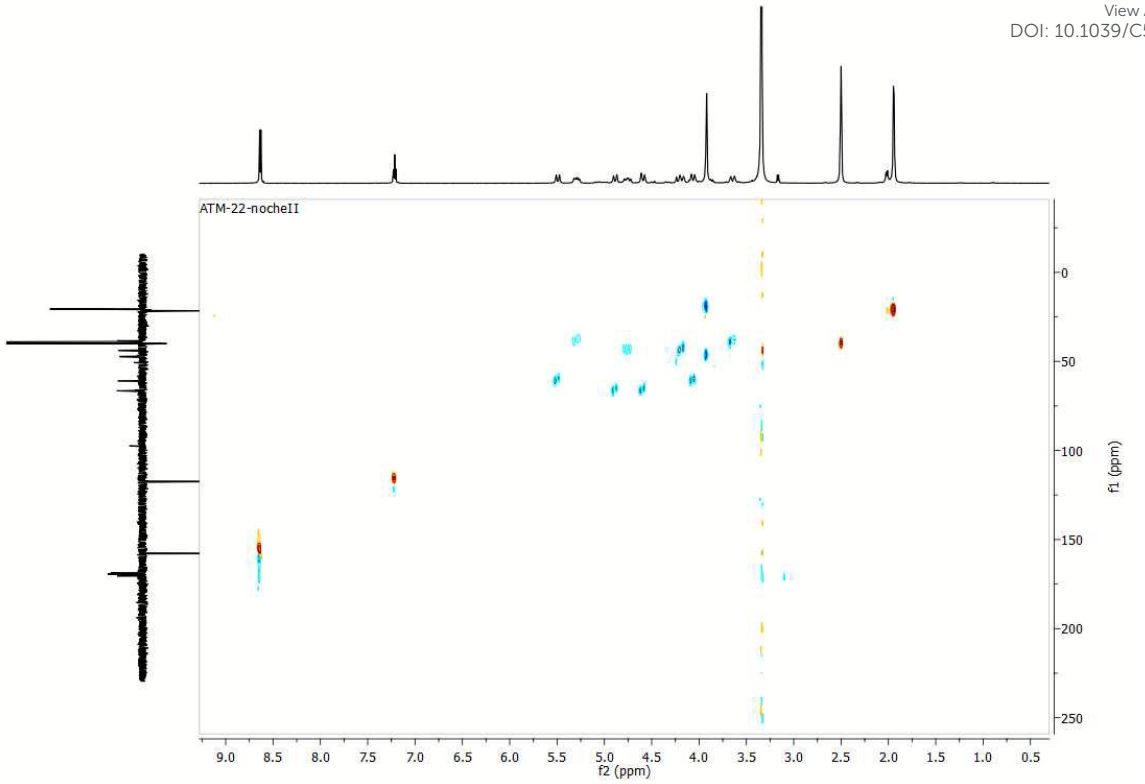

Figure S24. C,H-HSQC NMR of compound **8**

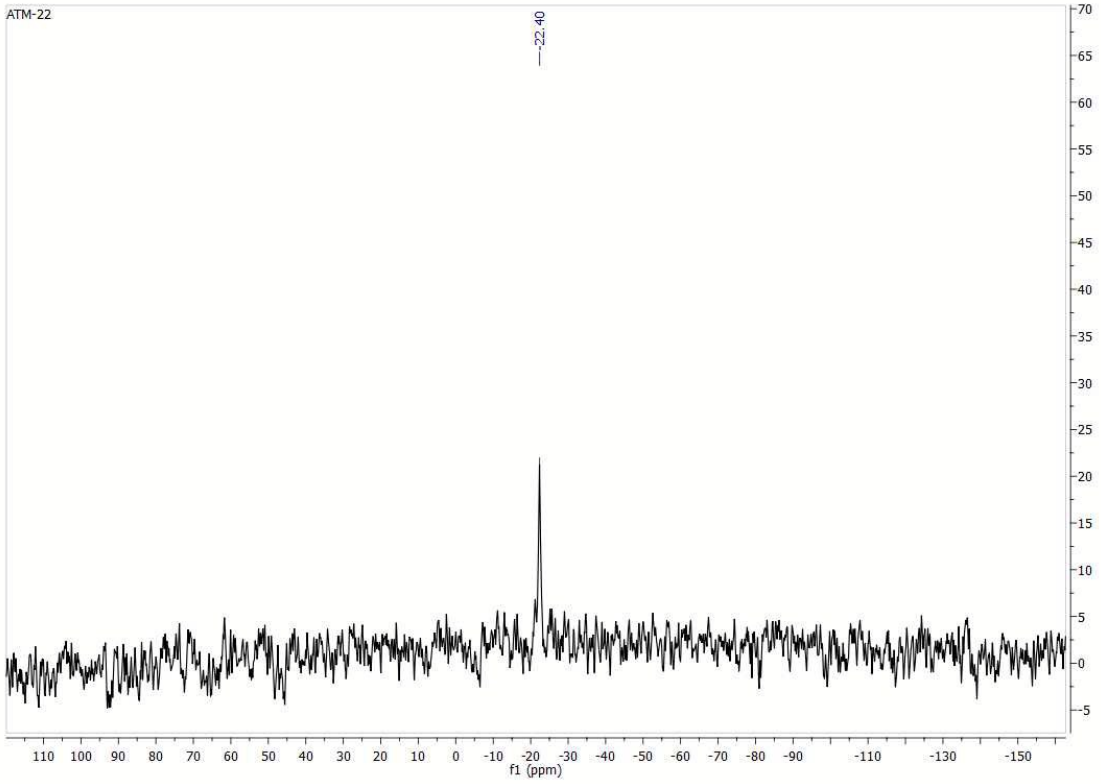

Figure S25. $^{31}P\{^{1}H\}$ NMR of compound **8**

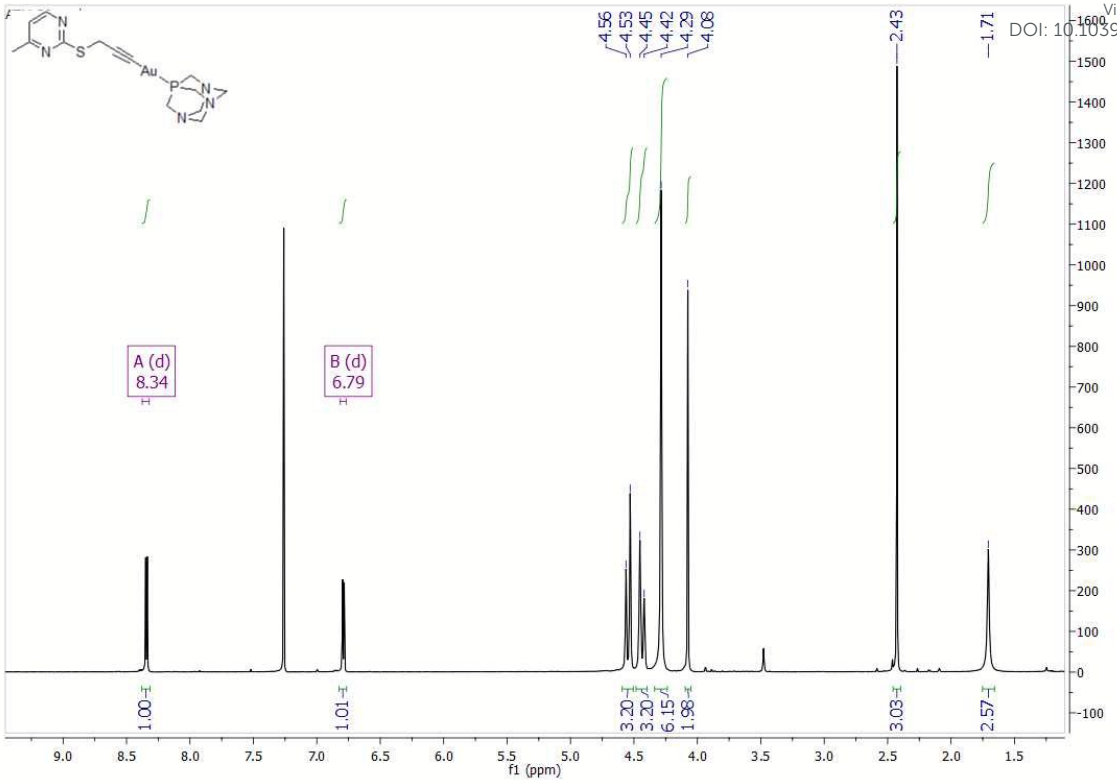

Figure S26.[1]H NMR of compound **9**

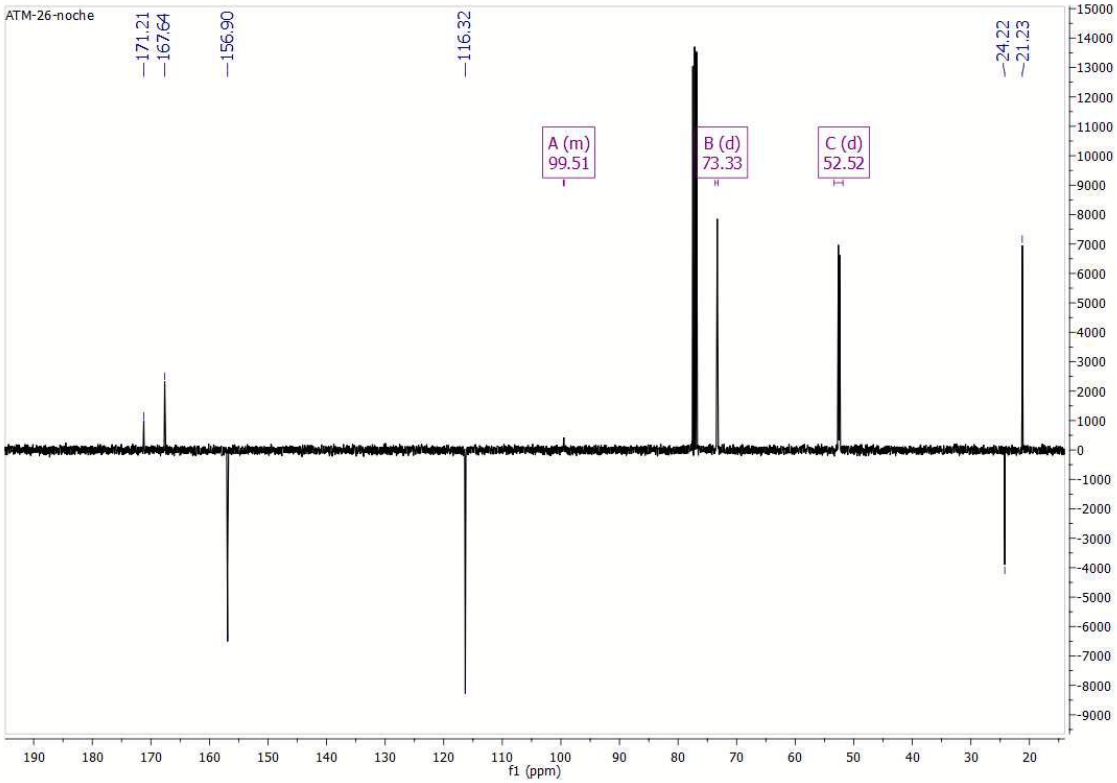

Figure S27. $^{13}C\{^{1}H\}$ NMR of compound **9**

View Article Online
DOI: 10.1039/C5DT01802A

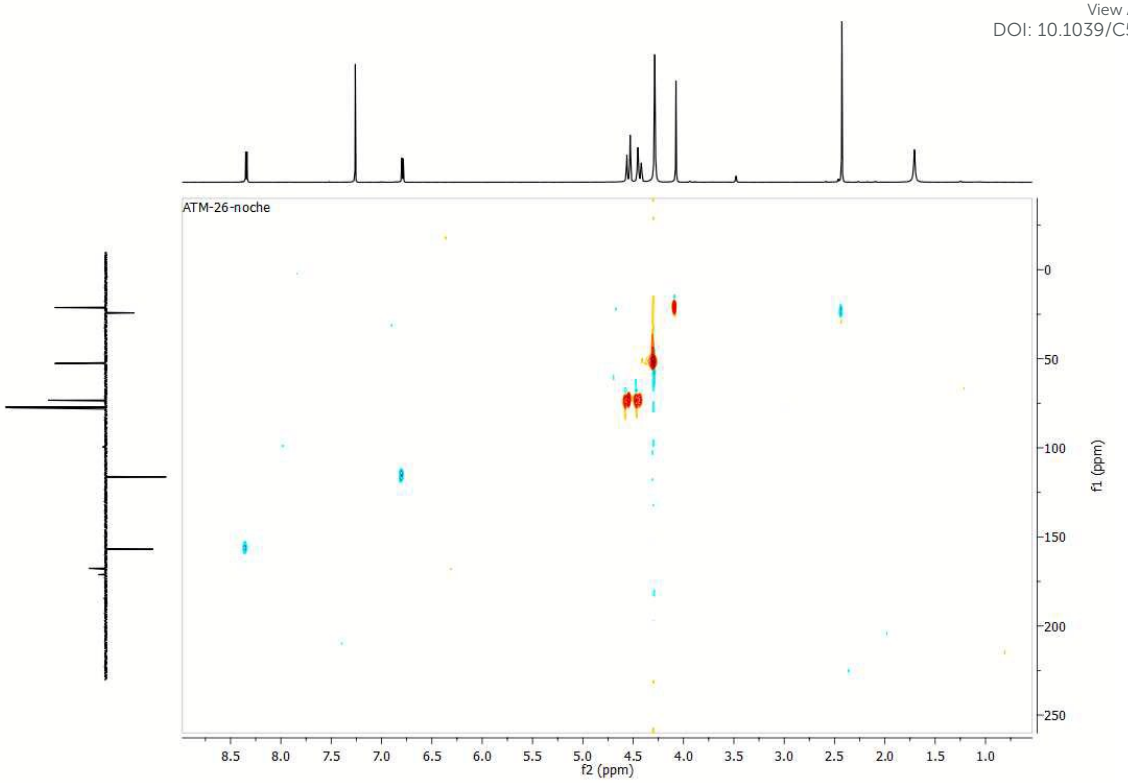

Figure S28. C,H-HSQC NMR of compound **9**

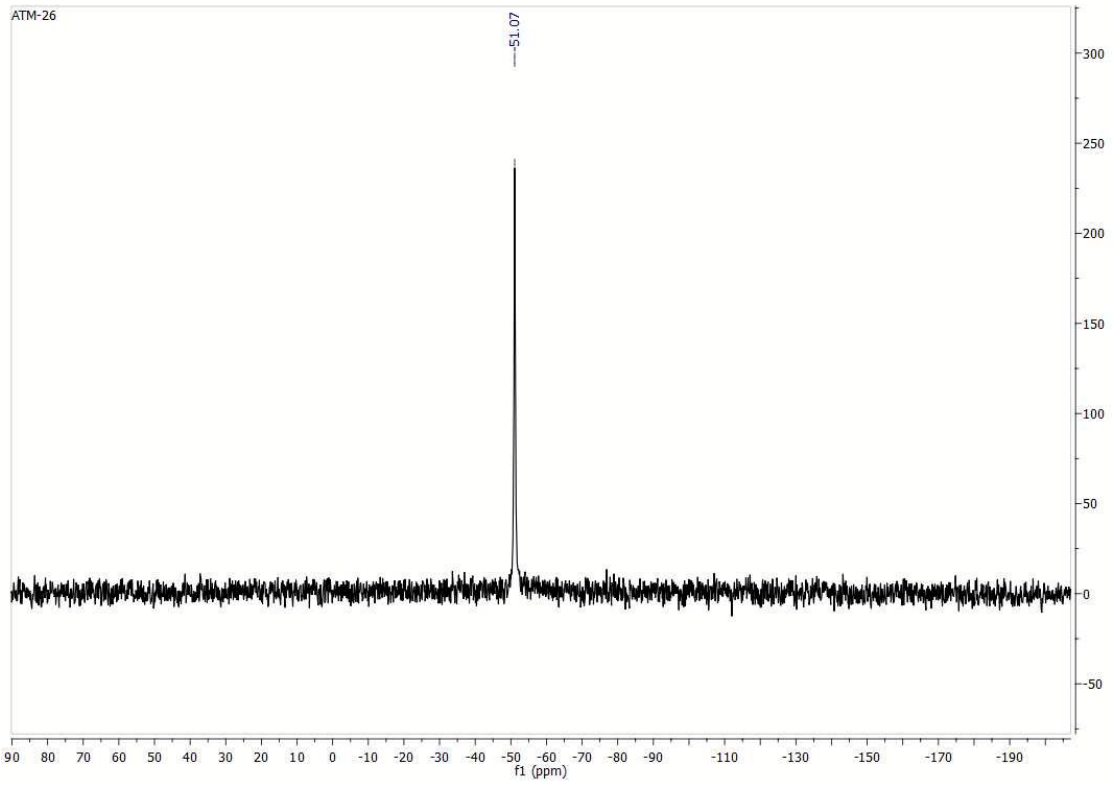

Figure S29. $^{31}P\{^{1}H\}$ NMR of compound **9**

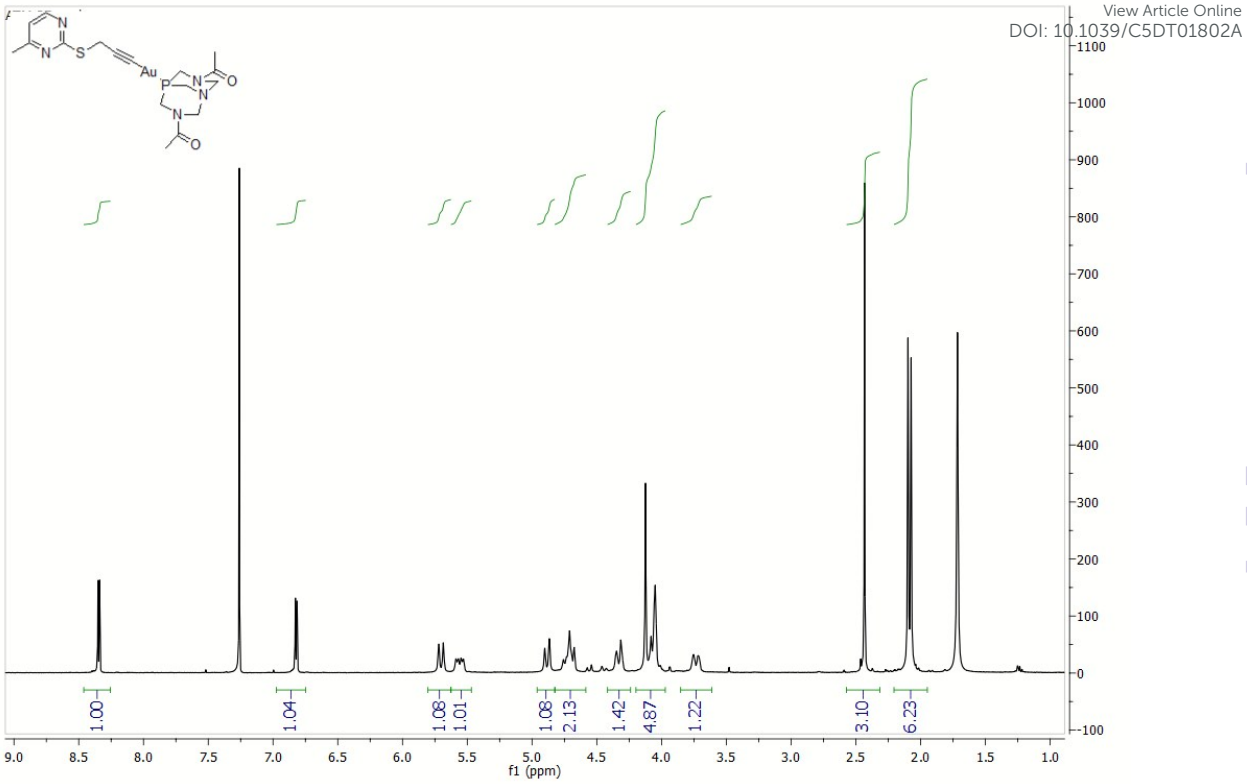

Figure S30. ^{1}H NMR of compound **10**

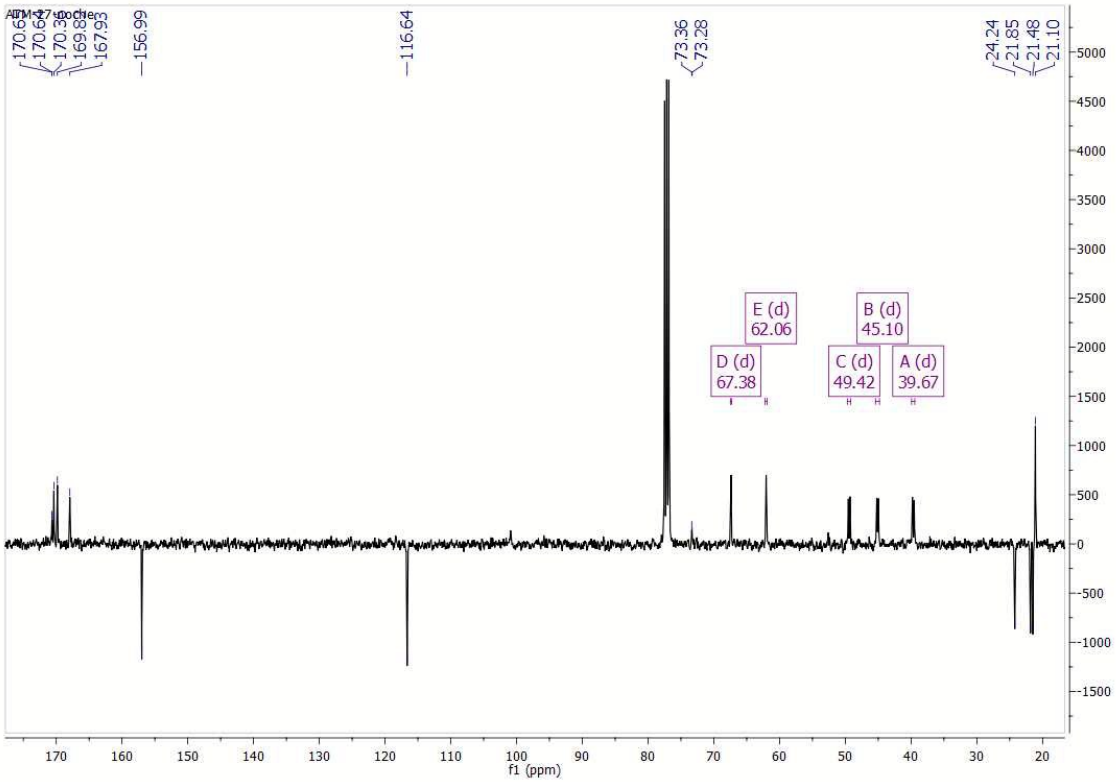

Figure S31. ^{13}C{^{1}H} NMR of compound **10**

View Article Online
DOI: 10.1039/C5DT01802A

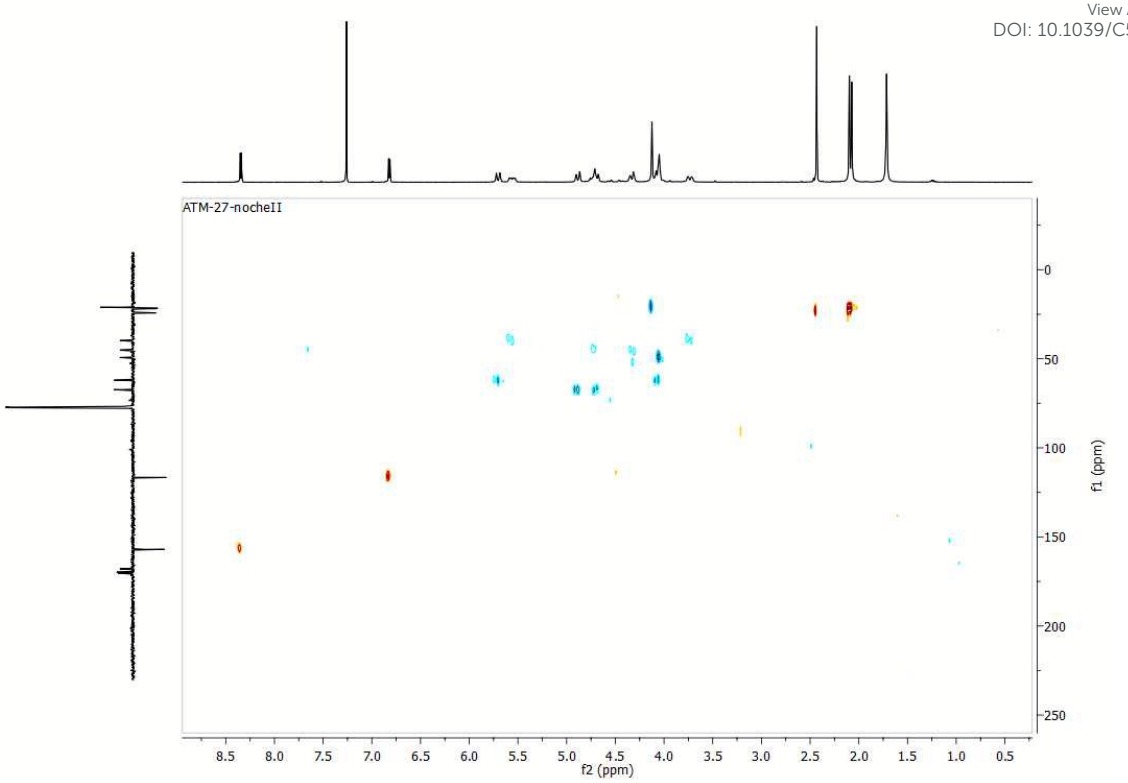

Figure S32. C,H-HSQC NMR of compound **10**

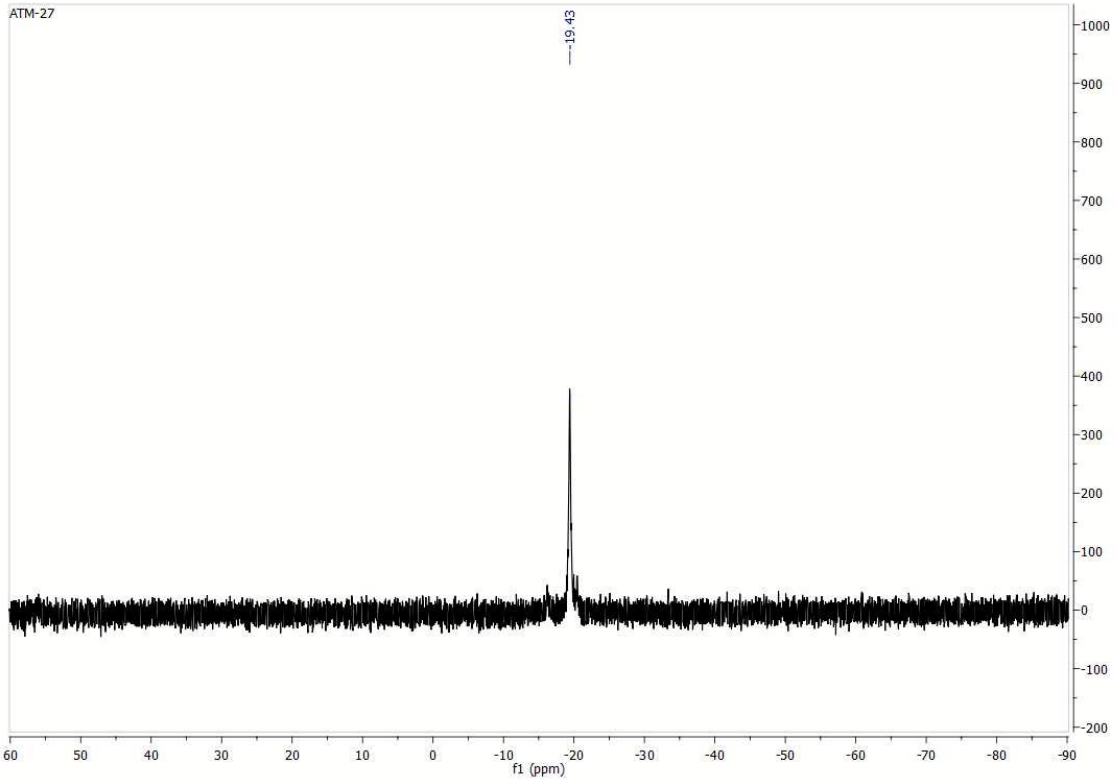

Figure S33. $^{31}P\{^{1}H\}$ NMR of compound **10**

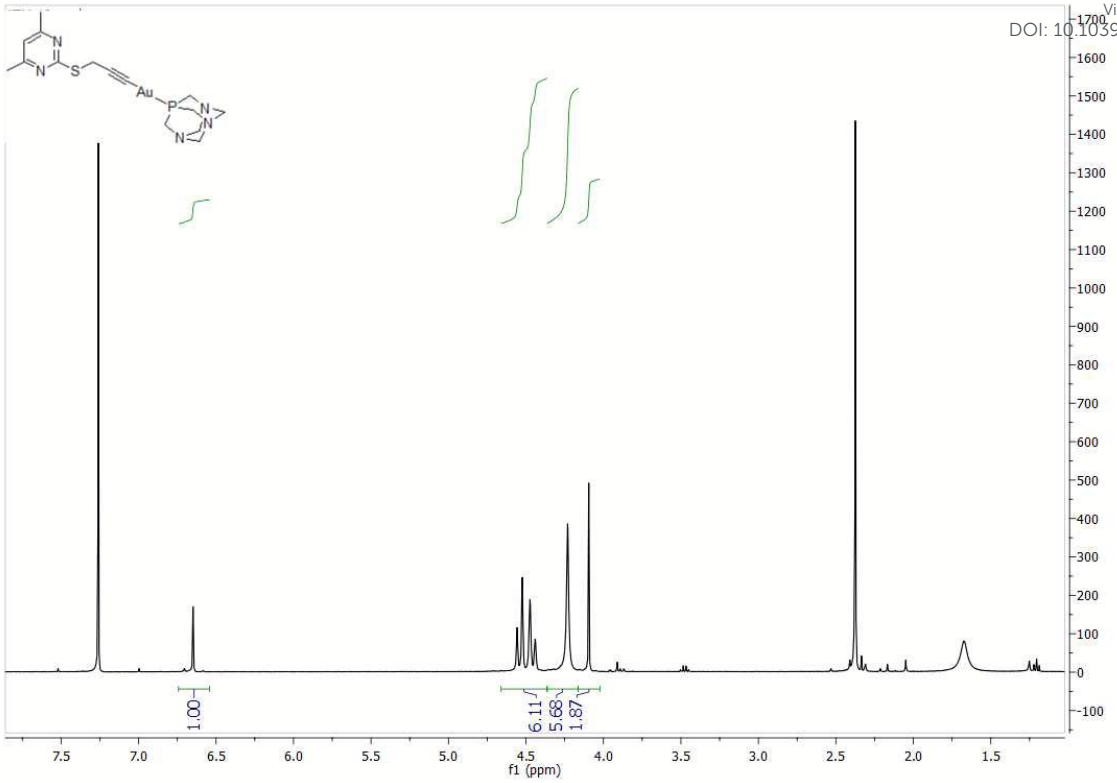

Figure S34. ^{1}H NMR of compound **11**

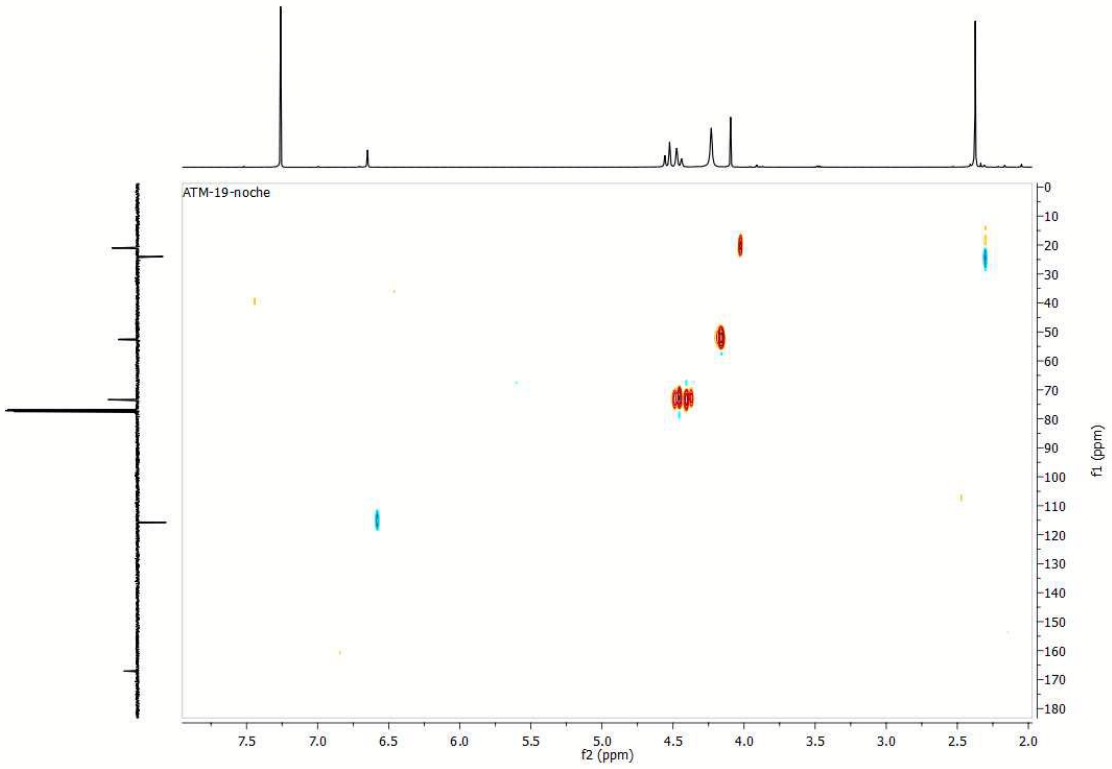

Figure S35. C,H-HSQC NMR of compound **11**

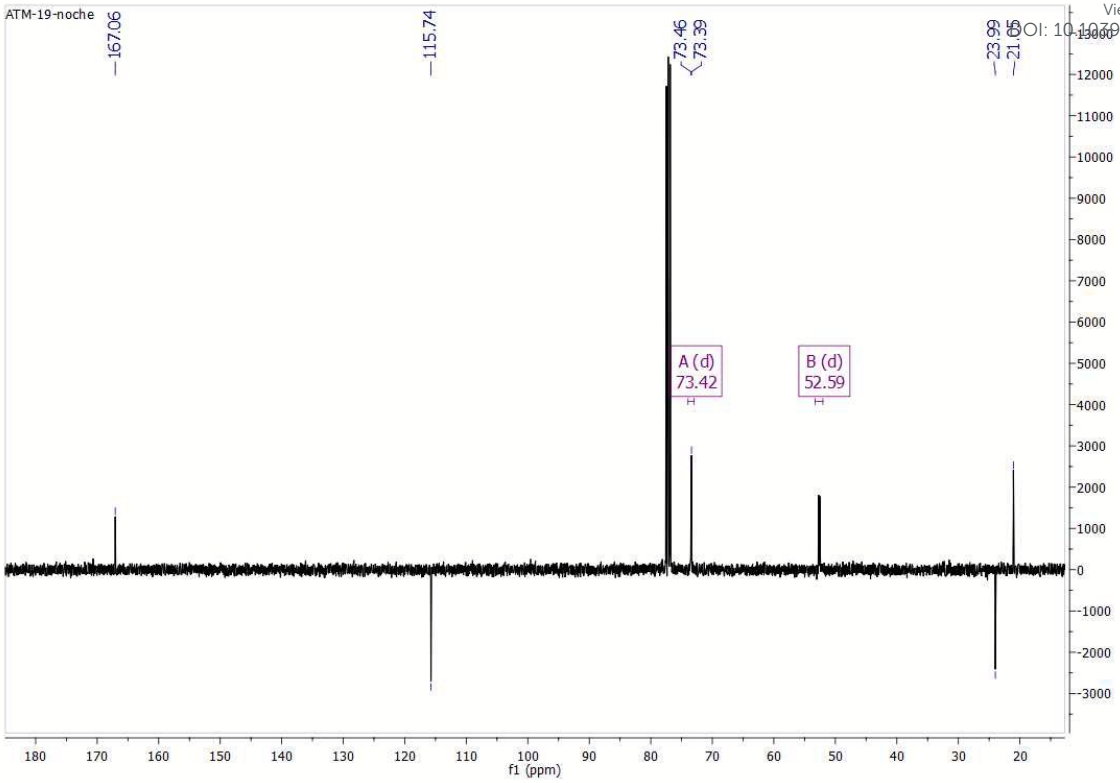

Figure S36. $^{13}C\{^{1}H\}$ NMR of compound **11**

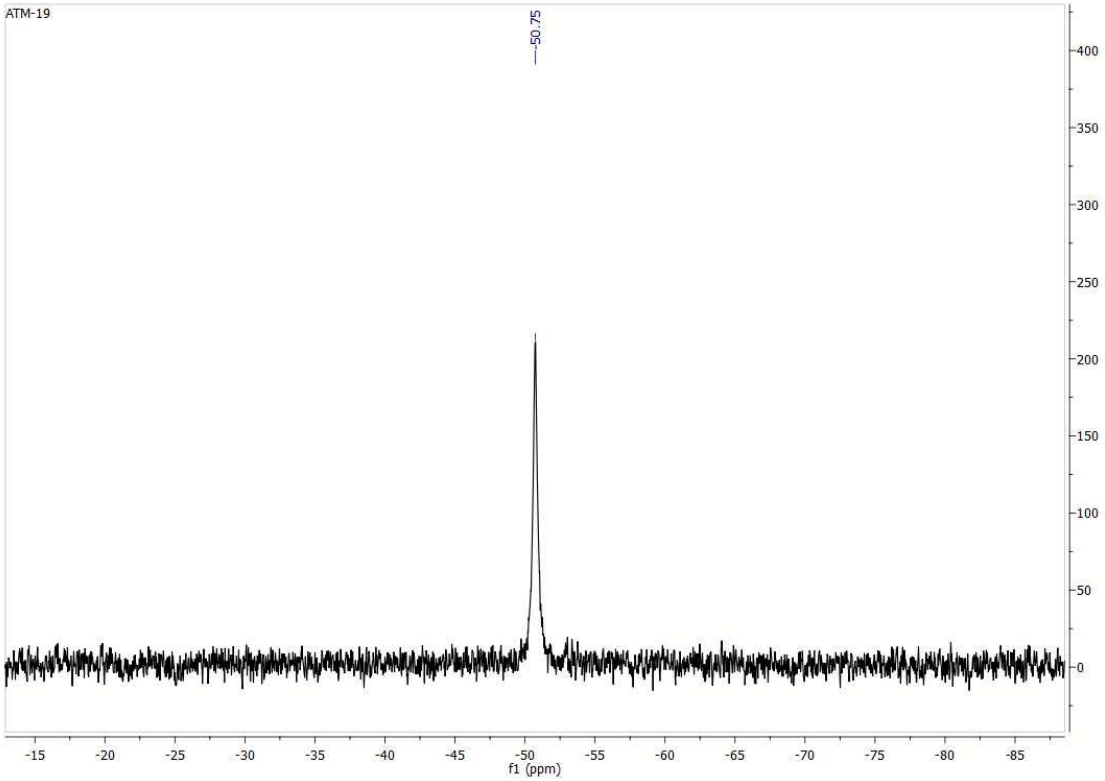

Figure S37. $^{31}P\{^{1}H\}$ NMR of compound **11**

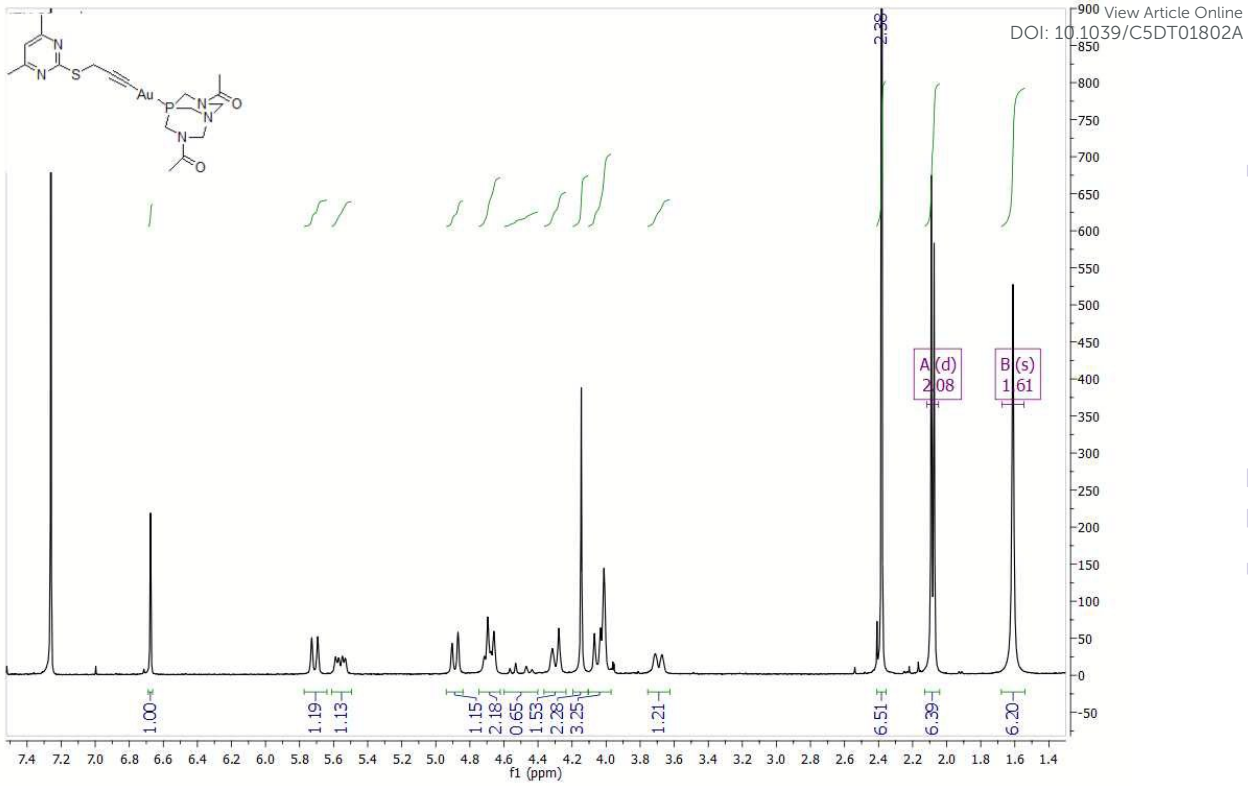

Figure S38. ^{1}H NMR of compound **12**

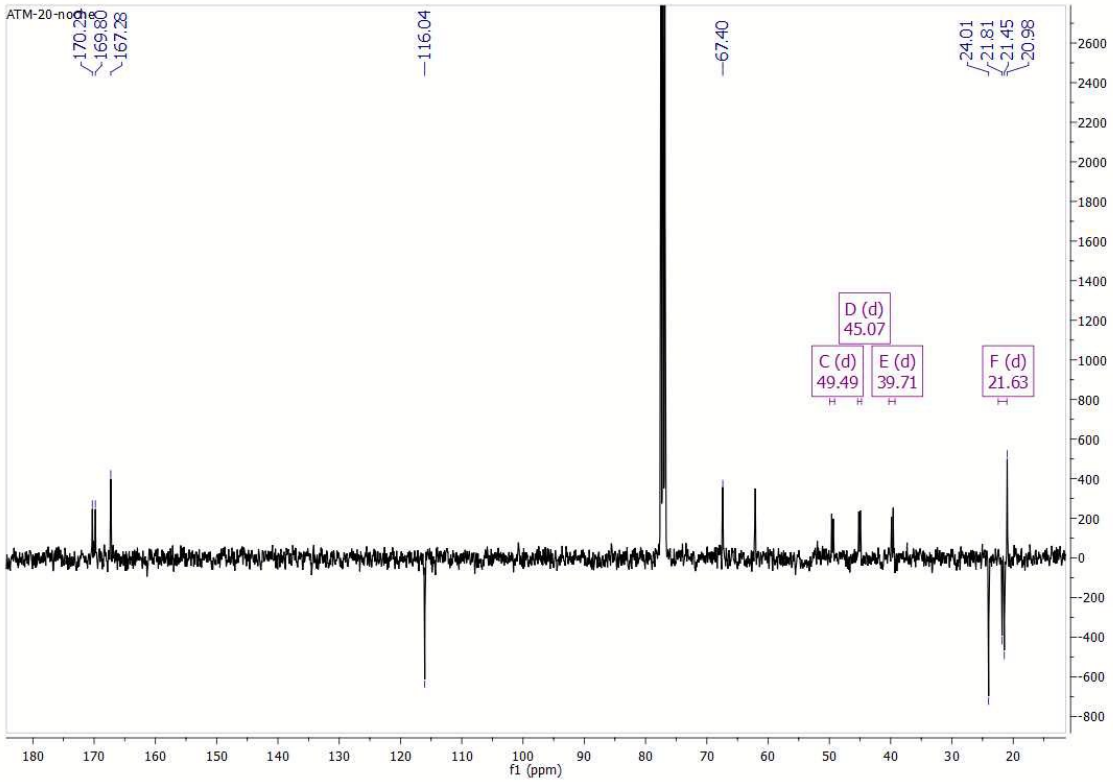

Figure S39. $^{13}C\{^{1}H\}$ NMR of compound **12**

View Article Online
DOI: 10.1039/C5DT01802A

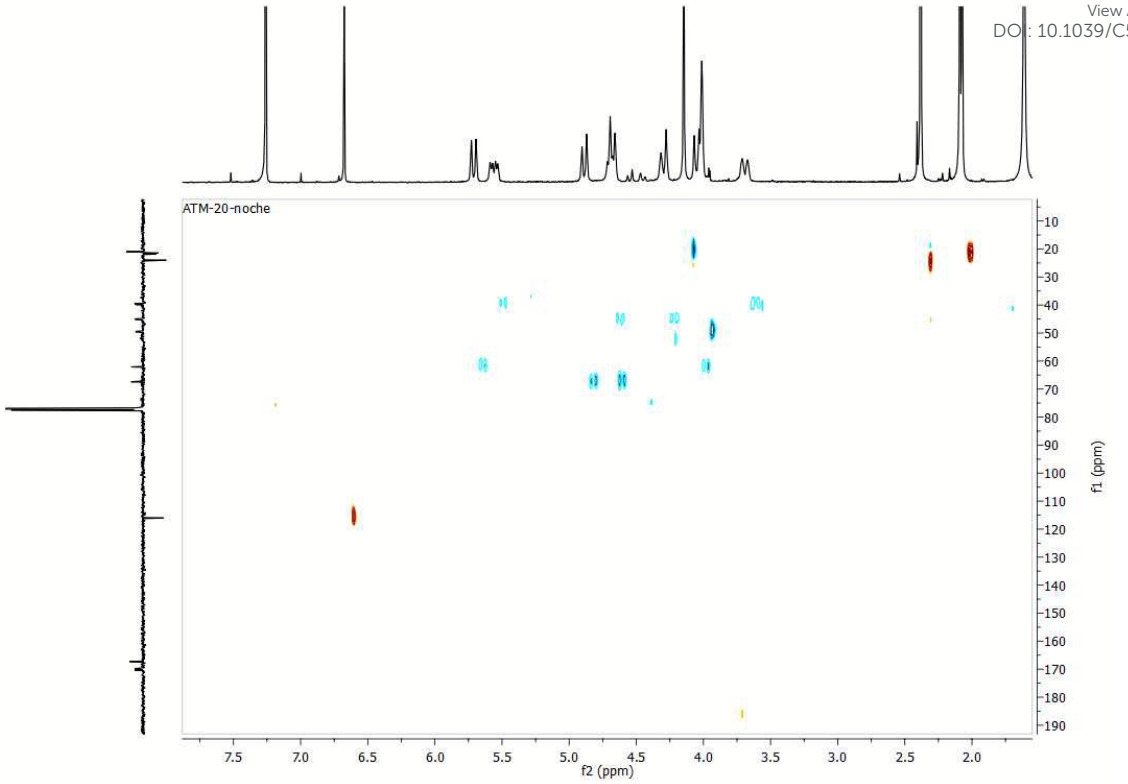

Figure S40. C,H-HSQC NMR of compound **12**

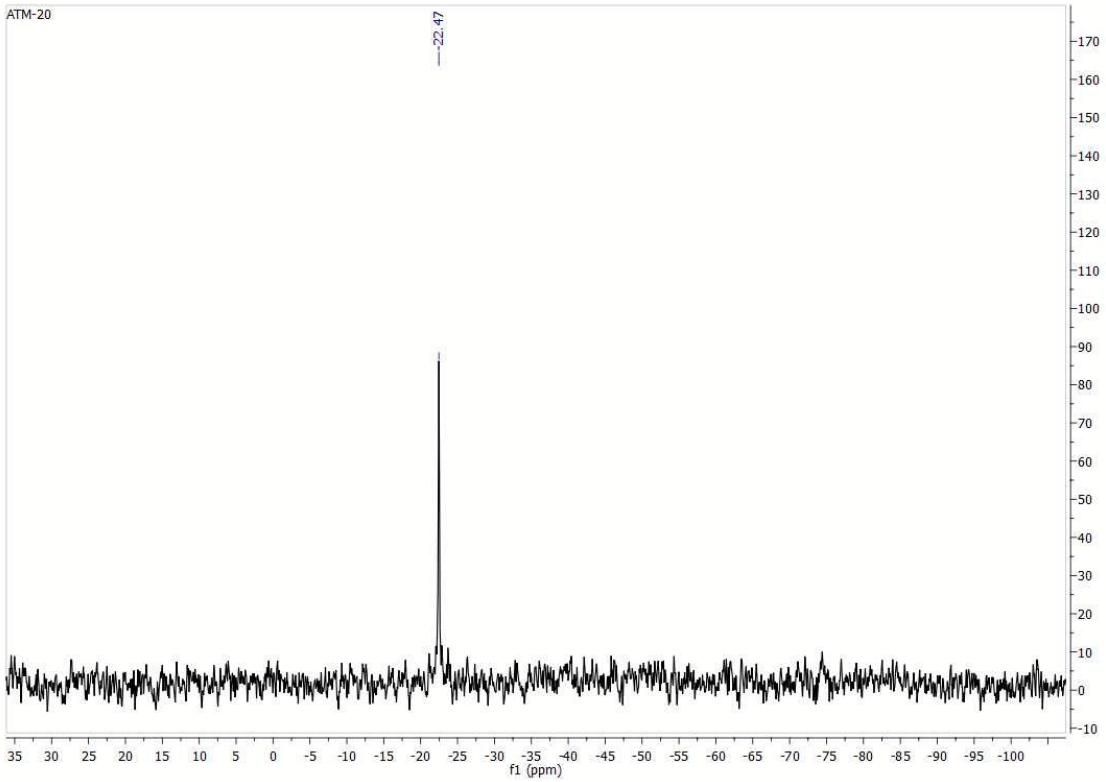

Figure S41. $^{31}P\{^{1}H\}$ NMR of compound **12**